University of Khartoum

Faculty of Engineering

Department of Mechanical Engineering

CFD Simulation of Axial Flow Turbine

A Thesis submitted in partial fulfillment of the requirements for the degree of Master of Science in Mechanical Engineering (Energy)

Prepared by:

Eng. Diaelhag Aisa Hamid Khalifa

Supervised by:

Dr. Ali Mohammed Ali Seory

March. 2008

Verse

قال تعالى:-

(يرفع الله الذين أمنوا منكم والذين أوتوا العلم درجات والله بما تعملون خبير)

صدق الله العظيم

سورة المجادلة الاية(11)

Dedication

To the soul of my mother

To my father

To all my family and teachers

Acknowledgements

I would like to express my gratitude to my supervisor, Dr. Ali Mohammed Ali for his close supervision and guidance throughout all stages of the thesis.

Gratitude is also extended to Dr. Mohammed Hashim (the head department of fluid mechanics) for his helpness and facilities offered to us.

Also I would like to thank all the technician staff of the Department of fluid mechanic in university of Khartoum for their help during the project.

Last but not least I would also like to thank my family and my friends for their support during the thesis.

Eng. Diaelhag Aisa Hamid

التجريد

هدفت الدراسة الى إستخدام حزمة تحسيب حركة الموائع المعروفة بال CFX , لتحليل سلوك السريان فى توربين محورى رد فعلى. المستخدم فى محطات توليد القدرة المائية ذات السمت المنخفض ومعدل التصريف العالى.

هذه الدراسة اشارت الى ان اداء الريشة التى تم تصميمها مقبول،وهذه الريشة يمكن إستخدامها فى توربين كابلن لانتاج القدرة المائية مع اجراء مزيدا من التحسينات التصميمية. هذه التحسينات تستخدم لتقليل تكون الدوامات فى مؤخرة الريشة (إتجاه السحب) وتمنع تكون الطبقة الجدارية فى مقدمة الريشة، وايضا هذه التحسينات تحتاج لمزيد من التحليل و مزيدا من الاختبارات وذلك باستخدام حزم تحسيب حركة موائع اخرى لاختبار النتائج.

وكذلك ركزت هذه الدراسة على ايجاد تغير مركبات السرعة والضغط باستخدام (المساحة الميحطية المتوسطة) من مدخل الريشة الى مخرجها كعوامل لتحليل سلوك السريان داخل الريش، واعطت هذه النتائج توقع جيد للسريان داخل الريش وهذا يقود الى قبول تصميم الريشة ويمكن استخدامها فى توربين كابلن.

Abstract

This study aims to use computational fluid dynamics software package (CFX) to study and analyze flow's behavior in an axial flow turbine. This turbine used in low head and high flow rate hydropower plant.

This study indicates that, performance of the designed blades is acceptable. These blades can be used in Kaplan turbine to produce a power with some addition design modification. These modifications can be made to reduce the tailing edge vortices (in suction side) of the blade and boundary layer forming in the leading edge of the blade. Also these modifications need furtherer analysis and more testing using another commercial CFD codes to investigate the results.

Also this study focused to found the variations of velocity components and the pressure by average circumferential area (ACA) from inlet to outlet of the blades and used as factors to analyzed the flow inside the blades, the results of this analysis shows a good prediction of the flow behavior inside the blades and this lead to acceptable blade design, which can be used in Kaplan turbine.

Table of Contents

List of Symbols

Symbol	Denotation	Unit
H	Head	m
Q	Volume flow rate	m^3/s
g	Gravitational acceleration	m/s^2
ρ	water density	Kg/m^3
η	Efficiency	-
P	Power	Kw
C_r	Axial of velocity	m/s
C_w	Whirl velocity	m/s
C	Absolute velocity	m/s
V	Relative velocity	m/s
U	Blade Speed	m/s
D	Diameter	m
r	Radius	m
m	mass flow rate	Kg/s
F	Force	N
ω	Angular velocity	rad/s
T	Torque	N.m
N	Rotational speed	R.P.M
Ns	Specific speed	-
σ	Cavitation factor	-
P	Pressure	Pa
$\boldsymbol{P'}$	Modified pressure	Pa
v	Kinematic viscosity	Kg/ms
U_i	mean velocity	m/s
u_i	velocity fluctuation	m/s
k	Turbulence kinetic energy	m^2/s^2
ω	Turbulence Frequency	-
μ	Dynamic viscosity	Kg/ms
$\boldsymbol{\mu_{eff}}$	Effective viscosity accounting for turbulence	Kg/ms
$\boldsymbol{\mu_t}$	Turbulence viscosity	-
$\boldsymbol{P_{kb}}$	Buoyancy production term	-
$\boldsymbol{y}$	The distance to the next surface	m
$\boldsymbol{CD_{k\omega}}$	The cross-diffusion term of equation	-
$F1$, $\boldsymbol{F_2}$	Blending factors	-

List of Figures

Chapter One

1.1 Introduction:

Hydro power plants generate about 41% of the electrical power produced in Sudan [1]. Even a small improvement of the hydrodynamic design and efficiency can contribute a great deal to the supply of the electric power in Sudan. The efficiency of a hydropower plant depends on a number of parameters, such as: Turbine efficiency, Draft tube efficiency and Generator efficiency. Most of the past studies have focused on the draft tube for increasing the efficiency of the plant, but a good draft tube design is not enough. Recent studies have shown that the efficiency improvement can also be realized by minor modification on the older design in the rest of the waterway i.e., in the draft tube, runner blades and spiral casing.

Previous studies have shown that there is potential for increasing unit performance by a moderate modification of such runner blades. Runner blades have been found to have an efficiency loss due to the runner losses.

A small increase in performance in these power stations represents a considerable economic value. This work will analyzed the flow field in the runner blades. This analysis is based on CFD simulations.

1.2 Motivation:

To be competitive and increase customer values, industry is always searching for better products at reduced design cycles and costs. For hydropower companies, small improvements of hydraulic turbines are of interest due to economical and safety aspects. New demands on the deregulated energy market make it also attractive to improve the turbines over a wide range of operating conditions. Furthermore, many of the turbines are old and in need of

rehabilitations and modifications. As a result, there is a great potential of improving hydraulic turbines and other related components using Computational Fluid Dynamics CFD.

The introduction of CFD in the area of hydraulic machine research is believed to increase a detailed knowledge of the flow inside the machines and to speed up the design procedure. This requires that the experience from CFD in this area is increased, which cannot be achieved without detailed experimental investigations to be used for comparisons. With sufficient experience of CFD in the area of hydraulic machine research, CFD will definitely be used in future hydraulic machine development.

A CFD programs solve the complicated Navier-Stokes equations governing fluids in motion by numerically integrating flow properties, such as velocity and pressure, over very small areas within a grid system throughout the flow field. Using an iterative procedure and starting with known hydraulic boundary conditions (e.g., head, velocity, and pressure at inlet and exit), the CFD program solves the equations over the entire grid system using an iterative procedure. Finally, the results are displayed to allow evaluation and to make alterations to enhance the design.

1.3 Organization of the Research:

This thesis includes six chapters; chapter one covers introduction, motivation, organization of the research and research objectives, chapter two covers the history of the hydraulic turbines, water turbine types, and previous studies for axial flow water turbine, chapter three covers theoretical background, and computational fluid dynamic (CFD), chapter four covers the Flow description, the governing equations of motion, turbulence models, and the geometry modeling, mesh generation and problem setup and solution. The results and

discussion were described in chapter five; the conclusion and recommendation are mentioned in chapter six.

1.4 Research objective:

The purpose of this research is:

- To study the flow field and global engineering quantities, especially pressure distribution, between the hub and shroud of an axial flow water turbine.
- The study focuses to Analyzed the flow inside the turbine runner and investigates to performance of turbine blade under CFX.10 software.
- Determine and choosing a CFD package for the purpose of turbine blade design and the meshing process of the fluid flow zone inside the turbines between blades.

Chapter Two

Literature Review

2.1 Introduction:

Hydraulic turbines are present in most countries and accounts today to about one fifth of the total electricity production in the world [2]. Furthermore, they are producing electricity with high efficiencies (up to *95%*) and with a minimum amount of pollution. In addition, they have great energy storing capabilities and are able to rapidly respond to daily changes in the electricity demand as well as being a pure base load, which are important features of the present deregulated energy market. The main disadvantages are, however, related to the local environment of the hydropower plant such as impaired fish migration and decreased natural habitats. In Sudan, hydropower is one of the major renewable energy resources [3].

2.2 History of hydraulic turbines:

The history of hydraulic machines is long, starting with the water wheels in order to extract mechanical energy from running water. The first hydraulic turbine, for practical purpose, was created in France 1827, by Fourneyron. It was an outward-flow turbine, where the water was directed from the centre to the periphery (axial to radial). After this innovation, the design of hydraulic turbines advanced rather rapidly. In United States 1849, Francis developed the inward-flow turbine, where the water instead moved from the periphery to the centre (radial to axial). At about the same time, the axial-flow turbine was invented in Europe, in which the flow both entered and leaved the runner in an axial direction. In California 1880, Pelton invented the bucket turbine, which was an improvement of the original water wheel, wherein a jet of water from a nozzle stroked the runner buckets in the free air. In the former Czechoslovakia 1913, Kaplan improved the axial-flow turbines with adjustable runner blades,

resulting in a great enhancement of the power generating characteristics. In England 1950, Deriaz developed the mixed-flow turbines, where the runner blades were mounted at an angle of the axis of rotations, compared to axial-flow turbines. In addition, there have been suggested a number of related turbines, as for example bulb-turbines which are horizontal axial-flow turbines. Today, the most commonly used turbines are the Pelton, Francis and Kaplan turbines, although they have been somewhat improved during the years [3]. In a hydraulic turbine, the water is directed to the turbine from the head water via the penstock and then discharged into the tail water, as illustrated in Fig (2.1). Inside the turbine, the waters energy is converted into mechanical energy through rotating shaft via the runner. The shaft rotates the rotor of the generator, where the mechanical energy is finally transformed into electricity and supplied to customers [4].

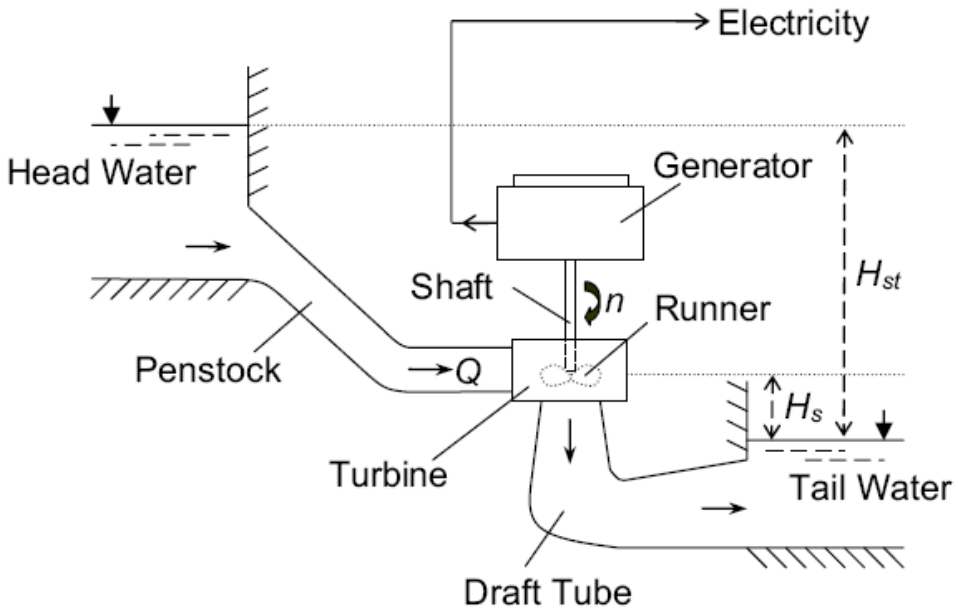

Fig (2.1): A representative sketch of a reaction turbine.

2.3 Types of Hydropower Turbines:

There are two main types of hydro turbines: impulse and reaction. The type of hydropower turbine selected for a project is based on the height of standing water—referred to as "head"—and the flow, or volume of water, at the site. Other deciding factors include how deep the turbine must be set, efficiency, and cost. Turbine selection is based mostly on the available water head, and less so on the available flow rate. In general, impulse turbines are used for high head sites, and reaction turbines are used for low head sites. Kaplan turbines are well-adapted to wide ranges of flow or head conditions, since their peak efficiency can be achieved over a wide range of flow conditions. Fig (2.2) represents the design and application charts.

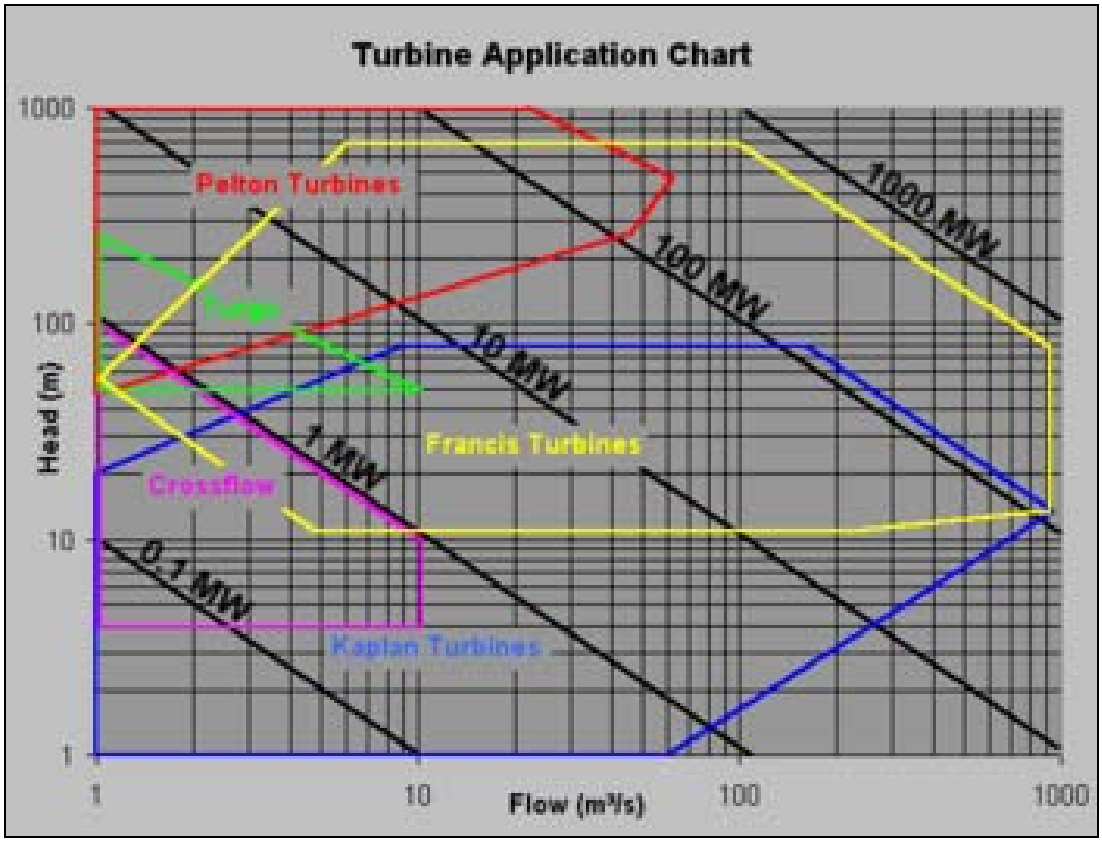

Fig (2.2): Typical turbine application chart [24].

2.3.1 Impulse turbines:

The impulse turbine generally uses the velocity of the water to move the runner and discharges to atmospheric pressure. The water stream hits each bucket on the runner. There is no suction on the down side of the turbine, and the water flows out the bottom of the turbine housing after hitting the runner. An impulse turbine is generally suitable for high head, low flow applications [5].

2.3.1.1 Pelton turbines:

Pelton turbines are impulse turbines where one or more jets impinge on a wheel carrying on its periphery a large number of buckets. Each jet issues water through a nozzle with a needle valve to control the flow as shown in Fig (2.3). They are only used for high heads from 60 m to more than 1000 m. The axes of the nozzles are in the plan of the runner. In case of an emergency stop of the turbine (e.g. in case of load rejection), the jet may be diverted by a deflector so that it does not impinge on the buckets and the runner cannot reach runaway speed. In this way the needle valve can be closed very slowly, so that overpressure surge in the pipeline is kept to an acceptable level (max 1.15 static pressure). As any kinetic energy leaving the runner is lost, the buckets are designed to keep exit velocities to a minimum.

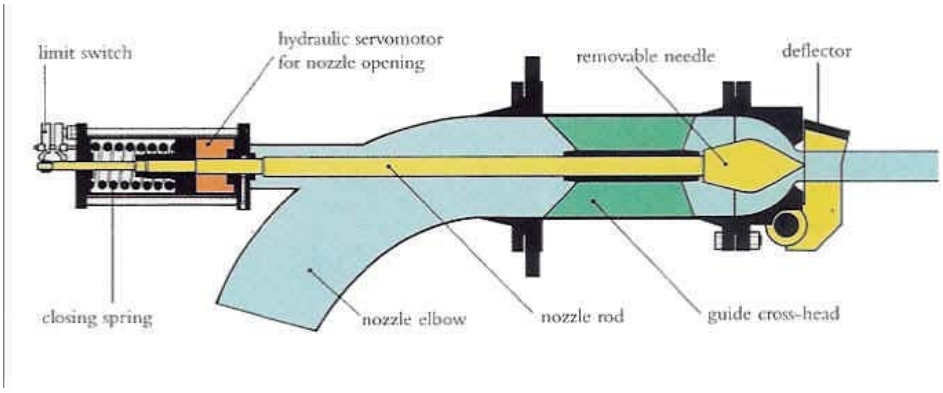

Fig (2.3): *Cross section of a nozzle with deflector*

One or two jet Pelton turbines can have horizontal or vertical axis, as shown in Fig (2.4). Three or more nozzles turbines have vertical axis see Fig (2.5). The maximum number of nozzles is 6 (not usual in small hydro).

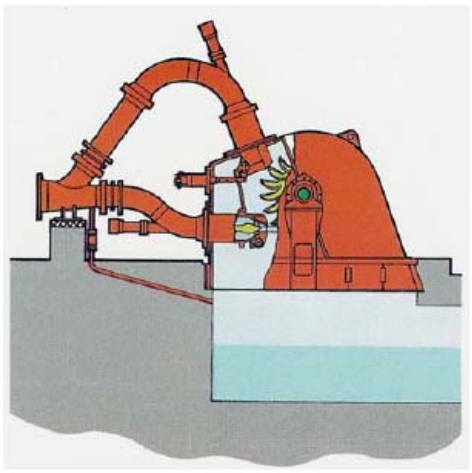

Fig (2.5):View of a two nozzles vertical Pelton

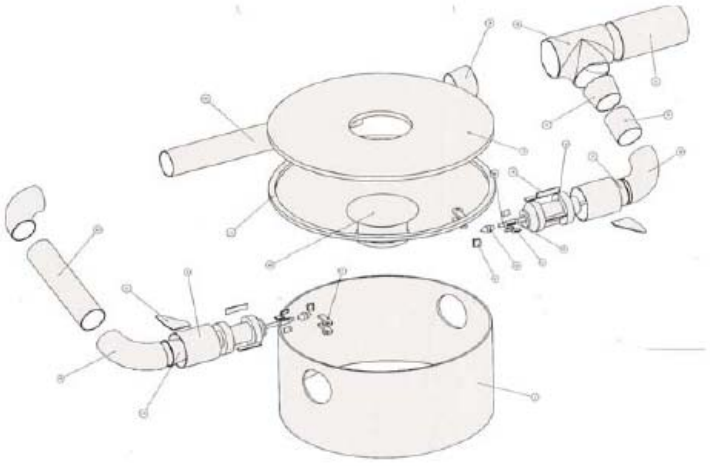

Fig(2.4): View of a two nozzles horizontal Pelton

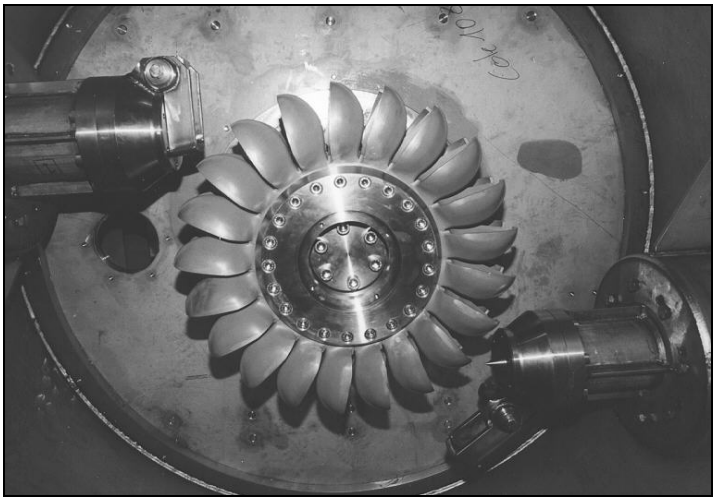

Fig (2.6): *Pelton runner*

The turbine runner as shown in Fig (2.6) is directly coupled to the generator shaft and shall be above the downstream level.

The turbine manufacturer can only give the clearance. The efficiency of a Pelton is good from 30% to 100% of the maximum discharge for a one-jet turbine and from 10% to 100% for a multi-jet one.

2.3.1.2 Turgo turbines:

The Turgo turbine can operate under a head in the range of 50-250 m. Like the Pelton, it is an impulse turbine, however its buckets are shaped differently and the jet of water strikes the plane of its runner at an angle of 20º. Water enters the runner through one side of the runner disk and emerges from the other as shown in Fig (2.7). It can operate between 20% and 100% of the maximal design flow.

The efficiency is lower than for the Pelton and Francis turbines. Compared to the Pelton, a Turgo turbine has a higher rotational speed for the same flow and head. A Turgo can be an alternative to the Francis when the flow strongly varies or in case of long penstocks, as the deflector allows avoidance of runaway speed in the case of load rejection and the resulting water hammer that can occur with a Francis.

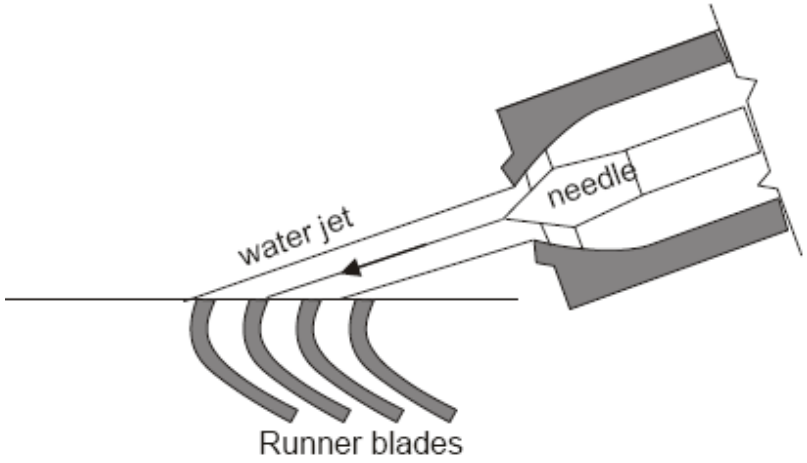

Fig (2.7): *Turgo turbine*

2.3.1.3 Cross-flow turbines:

This is an impulse turbine, also known as Banki-Michell is used for a wide range of heads overlapping those of Kaplan, Francis and Pelton. It can operate with heads between 5 and 200 m as shown in Fig (2.8).

Water enters the turbine, directed by one or more guide-vanes located upstream of the runner and crosses it two times before leaving the turbine.

This simple design makes it cheap and easy to repair in case of runner brakes due to the important mechanical stresses.

The Cross-flow turbines have low efficiency compared to other turbines and the important loss of head due to the clearance between the runner and the downstream level should be taken into consideration when dealing with low and medium heads. Moreover, high head cross-flow runners may have some troubles with reliability due to high mechanical stress.

It is an interesting alternative when one has enough water, defined power needs and low investment possibilities, such as for rural electrification programs.

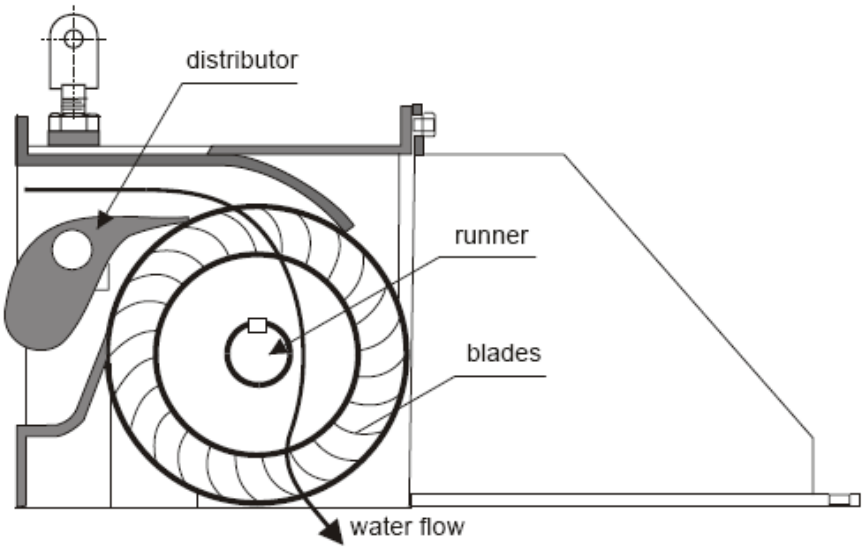

Fig (2.8): *Cross-flow turbine*

2.3.2 Reaction turbines:

A reaction turbine develops power from the combined action of pressure and moving water. The runner is placed directly in the water stream flowing over the blades rather than striking each individually. Reaction turbines are generally used for sites with lower head and higher flows than compared with the impulse turbines [6].

2.3.2.1 Francis turbines:

Francis turbines are reaction turbines, with fixed runner blades and adjustable guide vanes, used for medium heads. In this turbine the admission is always radial but the outlet is axial. Fig (2.9) shows a horizontal axis Francis turbine. Their usual field of application is from 25 to 350 m head. As with Peltons, Francis turbines can have vertical or horizontal axis see Fig (2.12), this configuration being really common in small hydro.

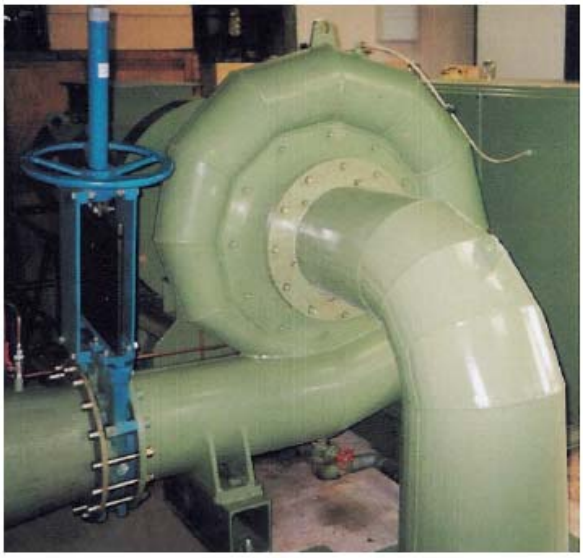

Fig (2.9): Horizontal axis Francis turbine

Francis turbines can be set in an open flume or attached to a penstock. For small heads and power open flumes were commonly employed, however nowadays the Kaplan turbine provides a better technical and economical solution in such power plants.

The water enters the turbine by the spiral case that is designed to keep its tangential velocity constant along the consecutive sections and to distribute it peripherally to the distributor. As shown in Fig (2.10), this one has mobile guide vanes, whose function is to control the discharge going into the runner and adapt the inlet angle of the flow to the runner blades angles. They rotate around their axes by connecting rods attached to a large ring that synchronize the movement off all vanes. They can be used to shut off the flow to the turbine in emergency situations, although their use does not preclude the installation of a butterfly valve at the entrance to the turbine. The runner transforms the hydraulic energy to mechanical energy and returns it axially to the draft tube see Fig (2.11).

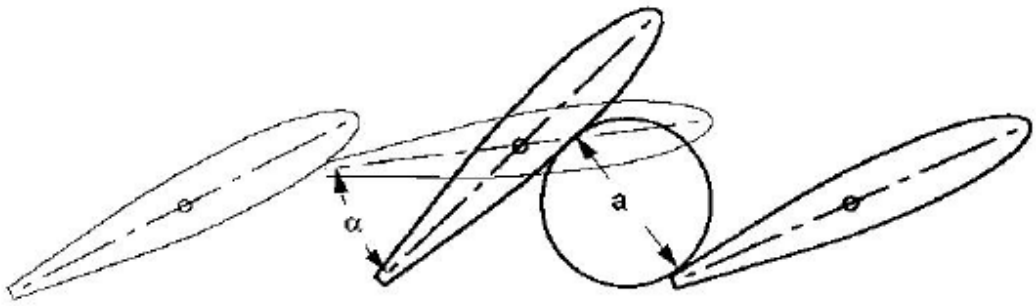

Fig (2.10): Guide vane functioning principle

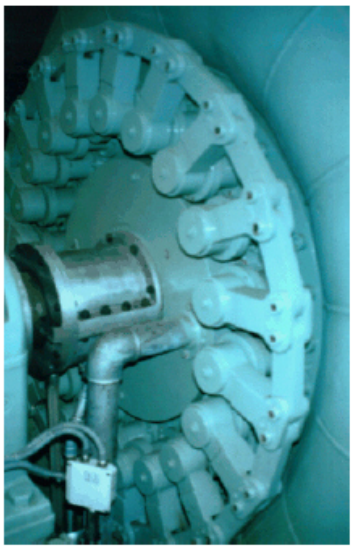

Fig (2.12): Horizontal axis Francis turbine guide vane operating device

Fig(2.11): Francis runner

Small hydro runners are usually made in stainless steel castings. Some manufacturers also use aluminum bronze casting or welded blades, which are generally directly coupled to the generator shaft.

2.3.2.2 Kaplan and propeller turbines:

Kaplan and propeller turbines are axial-flow reaction turbines; generally used for low heads from 2 to 40 m. The Kaplan turbine has adjustable runner blades and may or may not have adjustable guide-vanes. If both blades and guide-vanes are adjustable it is described as "double-regulated". If the guide-vanes are fixed it is "single-regulated". Fixed runner blade Kaplan turbines are called propeller turbines. They are used when both flow and head remain practically constant, which is a characteristic that makes them unusual in small hydropower schemes. The double regulation allows, at any time, for the adaptation of the runner and guide vanes coupling to any head or discharge variation. It is the most flexible Kaplan turbine that can work between 15% and 100% of the maximum design discharge. Single regulated Kaplan allows a good adaptation to varying

available flow but is less flexible in the case of important head variation. They can work between 30% and 100% of the maximum design discharge.

The double-regulated Kaplan illustrated in Fig (2.13) is a vertical axis machine with a spiral case and a radial guide vane configuration. The flow enters in a radial manner inward and makes a right angle turn before entering the runner in an axial direction see Fig (2.14). The control system is designed so that the variation in blade angle is coupled with the guide-vanes setting in order to obtain the best efficiency over a wide range of flows and heads. The blades can rotate with the turbine in operation, through links connected to a vertical rod sliding inside the hollow turbine axis.

Fig (2.14): *Kaplan runner*

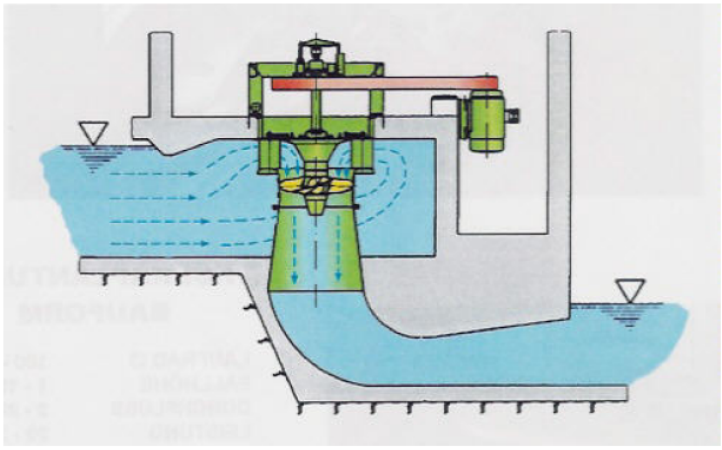

Fig (2.13): *Cross section of a double regulated Kaplan turbine*

Bulb units are derived from Kaplan turbines, with the generator contained in a waterproofed bulb submerged in the flow. Fig (2.15) illustrates a turbine where the generator (and gearbox if required), cooled by pressurized air, is lodged in the bulb. Only the electric cables, duly protected, leave the bulb.

Kaplan turbines are certainly the machines that allow the most number of possible configurations. The selection is particularly critical in low-head schemes where, in order to be profitable, large discharges must be handled.

When contemplating schemes with a head between 2 and 5 m, and a discharge between 10 and 100 m^3/sec, runners with 1.6 - 3.2 meters diameter are required, coupled through a speed increaser to a generator. The hydraulic conduits in general and water intakes in particular, are very large and require very large civil works with a cost that generally exceeds the cost of the electromechanical equipment.

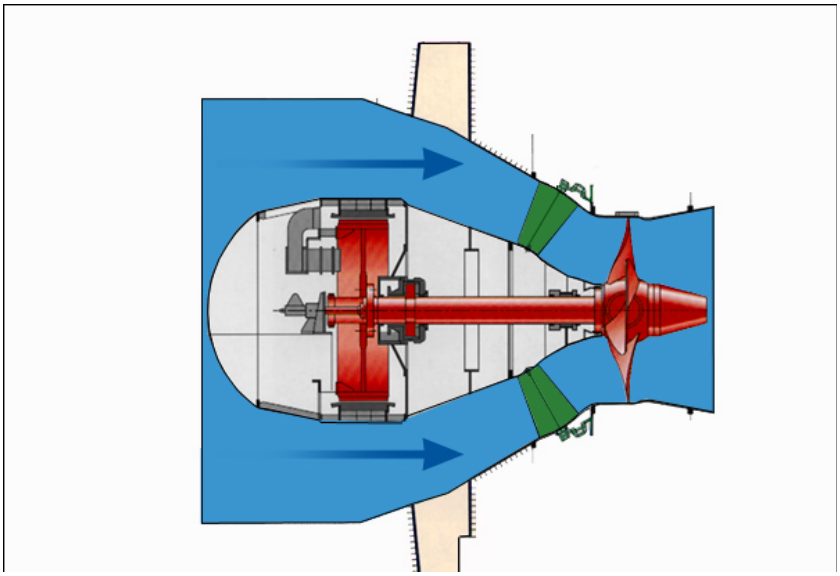

Fig (2.15): *Cross section of a double regulated Bulb turbine.*

2.4 Previous studies:

Performance characertristic of hydraulic machines are playing an important part in many engineeing applications, efforts have been done to improve the efficiency and performance characertristic of water turbine , the previous studies in the field of axial turbine are as below.

J.L.Grodon, et al:

Investigated many different types of turbine configurations available for low-head small hydro developments. Both axial flow (propeller) and radial flow (Francis) turbines used in about 10 different configurations, resulting in considerable difficulty in arriving at the most economical and appropriate unit

[7]. This short article outlines the steps used in conjunction with a computer program, to arrive at the types of units available for the site. The input data for the program includes the flow, desired number of units, the head, the system frequency, the tail water level, and the operating pattern in hours per annum at each flow, as obtained from a flow-duration curve. The program calculates the runner size and setting relative to tail water, speed, power output, provides charts showing turbine efficiency as a function of flow and power, the power plant kW/h output and the turbo-generator water-to-wire cost, for 10 different turbine configurations .The data is then screened for applicability to the site, and the inappropriate units discarded. The remaining units are compared, and two units are recommended, one based on maximum weight efficiency, and the other on minimum cost per kw/h output.

Two options are included in the program. One for the maximum allowable gearbox capacity (where used), and the other for the quality of the generator and SCADA system either industrial or utility. These options are explained further in this article. The program is limited to power plant capacity up to 30MW, turbine heads up to 30m, and the maximum flow per turbine up to 200m^3/s .Typical turbine-generator configuration, obtained from manufacture's brochures, are provided for all 10 generating units, A short site cost screening program is included within the turbine program, to be determine whether the site is worth further study.

Cook, et al:

Creation and Advance Hydropower Turbine System (AHTS) in 1994 by the US Department of Energy, Electric Power Research Institute, and the Hydropower Research Foundation. The Program's main goal is to develop "environmentally Friendly" hydropower turbines [8]. The program's first accomplishment was the development of conceptual design of new environmentally friendly turbines. In

order to do so, two contractors were competitively selected. The ARL/NREC team of engineers and biologists provided a conceptual design for a new turbine runner. The new runner has the potential to generate hydroelectricity at close to 90% efficiency. The Vioth team produced new fish-friendly design criteria for Kaplan and Francis turbines that can be incorporated in units during rehabilitation projects or in new hydroelectric facilities. These include the use of advanced plant operation, minimum gap runner, placement of wicket gates behind stay vanes, among others. The Vioth team also provides design criteria on aerating Francis turbines to increase dissolved oxygen content. Detailed reviews of the available literature studies, causation of injuries to fish, and available biological design criteria that would assist in the design of fish-friendly turbines were performed. This review identified a need for more biological studies in order to develop performance criteria to assist turbine manufactures in designing a more fish-friendly turbine.

Dr.J.D.Burton, et al:

Designed and tested a five bladed axial water turbine on the Oxford Canal. The turbine was tested with and without a diffuser to investigate the merits of water diffuser use [9].The diffuser design was scaled version of the Vortex wind diffuser, and the blades were untwisted of NACA 4412 profile. The turbine of 400mm diameter was tested on the front or narrow boat at varying loads and speed. A gear pump was used to load the turbine, from which pressure reading were used to calculate the torque .Water velocity and turbine rotational speed were recorded.The bare turbine gave an optimum power coefficient of 0.21+0.03.The optimum power coefficient for the diffuser augmented water turbine was 0.47+0.1, a power augmentation of 2.24 over the bare turbine. With the diffuser, the velocity of the water at the rotor was approximately 1.03 times the free stream velocity. Amore optimum blade selection is likely to give an increase in turbine performance.

H.Nilsson, et al:

Has been developed parallel multi-block finite volume CFD (computational fluid dynamic) code CALC-PMB (parallel multi-block) for computation of turbulent flow in complex domains and used for the computations of the flow through a Kaplan water turbine [10].The computations including the guide vanes and the runner, where the runner computations get .The inlet boundary condition from circumferentially averaged properties of guide vane computations. Four different operation conditions have been computed and the results from the computations are compared. The Computational results are in accordance with observations done by the turbine manufacture. This work if focused on tip clearance flow, which reduced the efficiency of the turbine by about 0.5%.

H.Nilsson, et al:

He studied experimentally the flow in the spiral casing distributer of the Holleforsen Kaplan water model. The measurements are an extension of the measurements for the turbine 99 and turbine 99-11 workshops. The velocity distribution in the spiral casing and distributor is measured with the LDV (Laser Doppler Velocimetry) technique. The work is collaboration between three in the Swedish Water Turbine Program [11].

Vesko Dijelic, et al:

Developed and tested four Kaplan turbine models developed for refurbishment of four hydropower plant was also tested by Turbo Institute using current meters for flow measurement .Model efficiency were scaled-up according to five common scale-up procedures (IEC995, Hutton, Ackeret, JSME and Fay-Kvyatkovskii) and compared to prototype tested efficiencies. The analysis of result showed that scale-up procedure from IEC995 recommendation give very realistic values of prototype efficiency on low head Kaplan turbine [12].

Gallus, et al:

Detailed experimental and numerical studies have been performance in subsonic [13], axial-flow turbine stage to investigate the secondary flow field, the aerodynamic loss generation, and the span wise mixing under a stage environment. The experimental study includes measurements of the static distribution on the rotor blade surface and the rotor exit flow field using three-dimensional hot-wire probe, which has high temporal and spatial resolution. Both steady and unsteady numerical analyses were performed with a 3D Navier-Stokes code for multiple blade rows. Special attention was focused on who well the steady multiple-blade- row calculation predicts the rotor exit flow field and how much the blade interaction affects the radial distribution of flow properties at the stage exit. Detailed comparisons between the measurement and steady calculation indicate that the steady multiple-blade-row calculation predicts the overall time-averaged flow field very well. However, the steady calculation does not predict the secondary flow ate the stage exit accurately. The current study indicates that passage vortex near the hub of the rotor is transported toward the mid-span due to the blade interaction effects. Also; the structure on the secondary flow field at the exit of the rotor is significantly modified by the unsteady effects. The time-averaged secondary flow field and the radial distribution of the flow properties, which are used for the design of the flowing stage, can be predicted more accurately with the steady calculation.

Wiriya Chanakul, et al:

Work aimed at [14] a program which is able to analyses and whether measurement of an effect water turbine for three types. They are Pelton Wheel, Francis and Kaplan turbine. As by the basic language and write by computer programs. The forming program was able to analyses and relative variables and also analyses of the three water turbine effective by insertion of all values some essential variables such as flow ate. The results of this analysis could by are

graph which can be improve in analysis stage for more effectiveness. It was concluded that the performance of this improving program, were effective in short-cut and reduce of all over-lapping works and could be accuracy-constant in measurements the time of all calculation about one minute of time and to be in error not exceed 0.186586%.

John Wiley, et al:

Investigates design optimization of axial flow turbine runner blade geometry [15]. In order to obtain a batter plane with good performance, a new comprehensive performance optimization procedure has been presented by combining a multi-variable multi-objective constrained optimization model with a (Q3).Diverse computation and performance procedure. With careful analysis of the inverse design of axial hydraulic turbine runner, the total hydraulic loss and the cavitations coefficient are taken as optimization objectives and comprehensive objective function is defined using the weight factors parameters of a newly proposed blade bound circulation distribution function and parameters describing positions of blade leading and tailing edge in the meridional flow passage are taken as optimization variables. The optimization procedure has been applied to the design optimization of a Kaplan runner with specific speed of 440. Numerical results show that the performance of design runner is successfully improved through optimization computation. The optimization model is found to be validated and it has the feature of good convergence. With the multi-objective optimization model, it is possible to control the performance of designed runner by adjusting the value of weight factors defining the comprehensive objective function.

Chapter Three

Theoretical Background and CFD

3.1 Introduction:

This chapter covers the theoretical background of the reaction turbines and brief description of the output power, diagram power, efficiencies, specific speed and cavitation. Overview of computational fluid dynamics also included. The reaction turbine is further subdivided into the Francis type, which is characterized by a radial flow impeller, and the Kaplan or propeller type, which is an axial-flow machine, each type of hydraulic turbine will be studied separately in terms of the velocity triangles, efficiencies, reaction, and method of operation [16].

In reaction turbine, water from the reservoir enters the turbine casing through penstocks. Hence, the total head is equal to pressure head plus velocity head. Thus, the water enters the runner or passes through the stationary vanes, which are fixed around the periphery of runners. The water then passes immediately into the rotor where it moves radially through the rotor vanes and exits from the rotor blades at a smaller diameter, after which it turns through 90^0 into the draft tube. The draft tube is a gradually increasing cross-sectional area passage. It helps in increasing the work done by the turbine by reducing pressure at the exit. The penstock is a waterway, which carries water from the reservoir to the turbine casing [16]. The inlet and outlet velocity triangles for reaction turbines are shown in Figures (3.1) and (3.2).

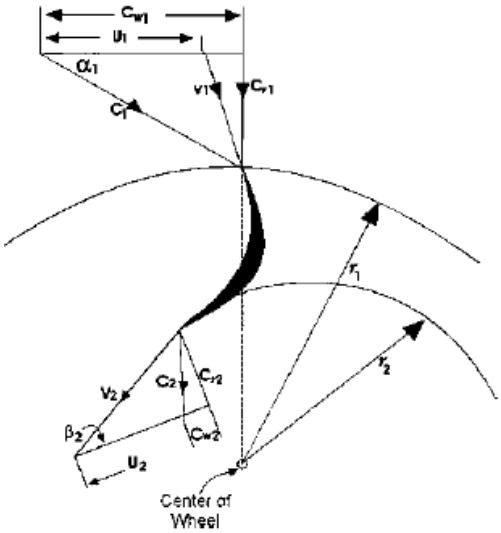

Fig (3.1): Velocity triangles for inward flow reaction turbine.

In an axial flow reaction turbine, also known as Kaplan turbine, the flow of water is parallel to the shaft. Fig (3.2) show the velocity triangles of an axial flow turbine, and are usually drawn at the mean radius, since conditions change from hub to tip. The flow velocity is axial at inlet and outlet, hence $C_{r1}=C_{r2}=C_a$ .C_1 Is the absolute velocity vector at angle $\propto_1$ to U_1, and V_1 is the relative velocity at an angle β_1. For maximum efficiency, the whirl component C_{w2}= 0, in which case the absolute velocity at exit is axial and then $C_2=C_{r2}$ see figure (3.2).

From the fig (3.1): From the inlet velocity triangle (subscript 1)

$$\tan \propto_1 = \frac{C_{r1}}{C_{w1}} \quad \text{..... (3.1)}$$

Also the absolute velocity at inlet, C_1 is

$$\sin \propto_1 = \frac{C_{r1}}{C_1} \quad \text{..... (3.2)}$$

And the Tangential velocity of the blade at inlet

$$U_1 = \frac{\pi D_1 N}{60} \quad \text{..... (3.3)}$$

And

$$\tan \beta_1 = \frac{C_{r1}}{(C_{w1} - U_1)} \quad \text{(3.4)}$$

Also the relative velocity of water at entrance

$$\sin \beta_1 = \frac{C_{r1}}{V_1} \quad \text{(3.5)}$$

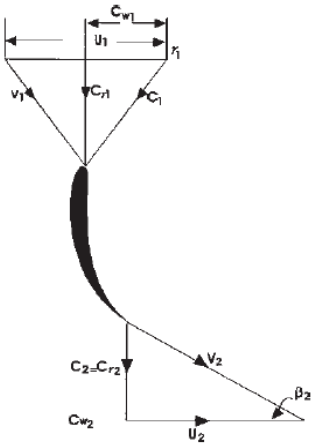

Fig (3.2): Velocity triangles for an axial flow hydraulic turbine

3.2.1 Power Output:

The moving force on the blade is defined as:

$$F = \dot{m}(C_{w1} - C_{w2}) \quad \text{(3.6)}$$

But the toque equation for Euler's Equation is

$$T = \dot{m}(C_{w1}r_1 - C_{w2}r_2) \quad \text{(3.7)}$$

For an axial flow water turbine $r_1 = r_2$, Then $U_1 = U_2$ *then* $U = \omega * r$

And the shaft power is

$$P_s = \omega * T \quad \text{(3.8)}$$

Or

$$P_s = 2\pi N * T \quad \text{(3.9)}$$

The Euler turbomachinery equation will give us the diagram power output

$$P = \dot{m} * U * (C_{w1} - C_{w2}) \quad \text{(3.10)}$$

3.2.1.1 Diagram power (P):

This is the power produced by the force of water acting on the rotor, it is reduced by losses before appearing as shaft power, the formula (3.10) depends upon the design of the turbine and involves analysis of the velocity vector diagram, means the theoretical power, based on momentum change in the fluid, the force on the vanes due to change in the fluid is $\boldsymbol{F = m * \Delta V}$ and these forces are vector quantities. The power of the force is always the product of force and velocity, the vector diagram constructed at inlet and outlet flow.

$$\boldsymbol{C_{r1} = C_{w1} * \tan \alpha_1 \ \ and \ \ C_1 = \frac{C_{r1}}{\sin \alpha_1}} \quad \text{..... (3.11)}$$

Also $\boldsymbol{C_{r1} = V_1 * \sin \beta_1}$ and $\boldsymbol{C_{w1} = \frac{C_{r1}}{\tan \beta_1} + U_1}$ ..... (3.12)

From these equation and velocity diagrams .The diagram power depends upon the inlet and outlet angle of guide vanes and runner blades, given by Eq (3.10).

3.2.2 Efficiency:

3.2.2.1 Hydraulic efficiency:

This is the efficiency with which water power is converted into shaft power output Eq (3.13) and is given by:

$$\eta_h = \frac{Diagram\ power\ output}{Fluid\ power\ available\ at\ inlet}$$

$$\boldsymbol{\eta_h = \frac{\dot{m}U(C_{w1} - C_{w2})}{\rho g H Q}} \quad \text{..... (3.13)}$$

3.2.2.2 Mechanical efficiency:

This is the efficiency with which the diagram power is converted into shaft power; the difference is the mechanical loss and is given by:

$$\eta_m = \frac{shaft\ power}{diagram\ power}$$

$$\eta_m = \frac{P_s}{\dot{m}U(C_{w1}-C_{w2})} \quad \text{..... (3.14)}$$

3.2.2.3 Overall efficiency:

This is the efficiency relating fluid power input to the shaft power output and is given by:

$$\eta_o = \frac{shaft\ power}{Fluid\ \ power\ available\ \ at\ inlet}$$

Or $$\eta_o = \eta_h * \eta_m \quad \text{.....} \quad (3.15)$$

$$\eta_o = \frac{\dot{m}U(C_{w1}-C_{w2})}{\rho gHQ} * \frac{P_s}{\dot{m}U(C_{w1}-C_{w2})} = \frac{P_s}{\rho gHQ} \quad \text{..... (3.16)}$$

The equation of hydraulic efficiency, Eq (3.13) expresses the power transfer to the runner is further exposed to additional losses before the resulting shaft power (Ps) is transferred to the generator shaft. These losses are composed of mechanical friction in the bearing and stuffing boxes, viscous friction from the fluid between the outside of the runner and the covers of the reaction turbines.

Through the space between the covers and the outside of the runner a leakage flow also passes according to the clearance of the labyrinth seals, from the inlet rim to the suction side of the runner. Some energy is also required for operation of the turbine governor, tapping water for sealing boxes, ejectors and cooling of bearing and the governor oil. On account of all these losses the turbine efficiency is always lower than the hydraulic efficiency. Therefore, at the discharge (Q) and the power (P) transferred from the turbine shaft to generator shaft, the efficiency is defined in Eq (3.16). Usually the maximum efficiency

point which is represented by the best operating condition, is reaching values of say $\eta = 0.85\ to\ 0.90$ of the larger and best reaction turbines.

3.3 Specific Speed:

It is the quantity giving the relation between N, P and H; the values apply to a range of geometrically smeller turbo machines of all sizes. The specific speed Ns of a turbine characterizes the turbine's shape in way that is not related to its size showing fig (3.3) allows a new performance design to be scaled from an existing design of known performance. The specific speed is also the main criteria for matching a specific hydro site with the correct turbine type. The specific speed of a turbine can also be defined as the speed of an ideal geometrically similar turbine, which yields one unit of power at one unit of head. The specific speed of a turbine is given by the manufacture (along with other ratings) and always refers to the point of the maximum efficiency. This allows accurate calculations to be made of the turbine's performance for a range heads and flows.

$$N_s = \frac{N*\sqrt{P}}{H^{5/4}} \quad \text{..... (3.17)}$$

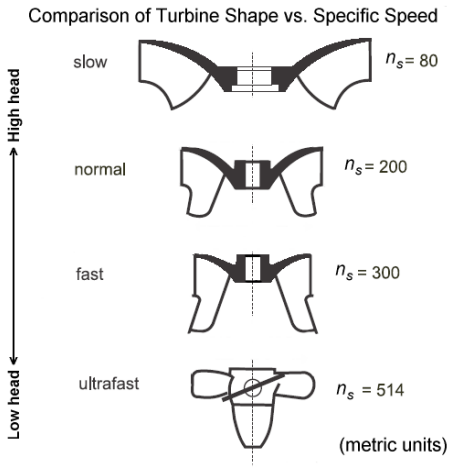

Fig (3.3): Comparisons of turbine Specific Speed [25].

3.4 Cavitation:

The presence of voids in the liquid has a damaging effect on marine and hydraulic turbine propellers [17]. Cavitation is the rapid vaporization and condensation process of liquid. It normally occurs when the local pressure in the liquid drops to or below vapor pressure, and with nuclei present in the liquid vapor cavities (bubbles) are formed. These bubbles grow within the vapor pressure region and then become unstable and collapse as they travel to areas with higher pressures. The collapse of bubbles can sometimes be violent and cause noise, vibrations, pressure fluctuations, erosion damage to solid surfaces, and loss of efficiency or flow capacity. Cavitation damage can occur as a result of high-pressure shock waves (that can reach up to 10^6 psi) or high-velocity microjets shooting through the center of the bubble creating a local pit to the bubble's adjacent solid boundary [17]. Cavitation can also reduce turbine efficiency.

A widely used non-dimensional cavitation parameter, σ , can be defined as the ratio of operating pressure conditions to the available gross hydraulic head, H, on the turbine runner. This is expressed as

$$\sigma = \frac{H_{atm} - H_s - H_v}{H} \quad \text{..... (3.18)}$$

Where: H_{atm} the absolute atmospheric pressure.

H_s the turbine runner setting relative to tail water level.

H_v is the vapor pressure.

To avoid cavitation at a hydro plant, its operational σ must be higher than its critical value, σ_{cr}, where σ_{cr} is when cavitation starts to be damaging to the turbine. Cavitation can also be minimized by properly designing the runner geometry to minimize parameters governing cavitation, which include high

velocity/low pressure zones, surface irregularities, abrupt changes in flow direction, and location or submergence.

3.5 Overview of Computational Fluid Dynamics (CFD):

With the rise in complexity of engineering problems and the need to minimize costs while increasing productivity, the use of computer-aided simulation has become widespread. Experiments both on site and in the laboratory, although of great importance, cannot give complete information on their own, not to mention the high. Costs involved. Numerical simulation combined with measurements is therefore most likely to constitute the basis for the analysis and design of marine current devices and farms. This section overviews one technique which will be of great use in this regard: Computational Fluid Dynamics (CFD) [18], was used extensively for this write-up because of its precise and concise treatment of the subject.

3.5.1 What is Computational Fluid Dynamics?

Computational Fluid Dynamics (CFD) is the analysis of systems involving fluid flow, heat transfer and associated phenomena such as chemical reactions by means of computer-based simulation [18]. It is computationally-based and enables the creation of a 'virtual prototype' of a system or device that is to be analyzed and then applying physics and chemistry to the model, predictions are made as to how the system will perform. Some examples are:

- Aerodynamics of wind turbine blades: lift and drag
- Heating and ventilation in buildings
- Flow in the ocean and rivers
- Weather prediction
- Cooling of equipment in electric circuits
- Blood flow through arteries and veins

From the 1960s onwards the aerospace industry integrated CFD techniques into the design, R&D and manufacture of aircraft and jet engines. More recently the methods have been applied to the design of internal combustion engines, combustion chambers of gas turbines and furnaces [18]. Increasingly CFD is becoming a vital component in the design of products and processes. The costs involved in investing in CFD, though not cheap, are lower compared with high quality experimental facilities. For instance the costs involved in designing, building and commissioning of a purpose built wave tank for wave energy device testing far outweigh that involved in the CFD analysis of the problem. Other advantages include:

- Ability to study the problem at a larger scale than the tank can handle
- Substantial reduction of time and effort
- Higher level of detail of the interaction between the device and the wave resource can be examined
- Ability to test the device under hazardous conditions at and beyond their normal performance limits (e.g. safety studies and accident scenarios).

3.5.2 How does a CFD code work?

The basic principle of CFD is to split the domain that is to be analyzed into small elements. For each of these elements, a set of partial differential equations are solved, which approximates a solution for the flow in order to achieve the conditions of conservation of mass, momentum and energy. The three basic equations are solved simultaneously with any additional equations implemented in a particular model to obtain the flow velocities, pressure and, therefore, any derived quantities.

For easy access to their solving power all commercial CFD packages contain three main elements:

(i) A Pre-processor

(ii) A Solver

(iii) A Post-processor

A brief description of their respective functions is as follows:

3.5.2.1 Pre- processor:

The pre-processor serves as a source of input of the flow problem to the CFD program by means of an operator interface. This is then transformed into a form suitable for the solver. The user activities at the pre-processing stage involve:

- Definition of the geometry of the region of interest.
- Mesh or Grid generation: the sub-division of the domain into a number of smaller, non-overlapping sub-domains.
- Selection of the physical and chemical phenomena that is to be modeled.
- Definition of fluid properties.
- Specification of the appropriate boundary conditions.

The solution to the flow problem (velocity, pressure, temperature etc.) is defined at nodes inside each cell. Generally, the larger the number of cells in the domain the better the solution accuracy. Both the accuracy of the solution and its costs in terms of necessary computer hardware and calculation time are dependent on the fineness of the grid. It is good practice to have non-uniform meshes: finer in areas where large variations occur from point to point and coarser in regions with relatively little change.

Over 50 % of the time spent in industry on a CFD project is devoted to the definition of the domain geometry and grid generation [18]. Currently almost all major codes now include their own CAD-style interface facilities to import data from surface modelers and mesh generators such as PATRAN, GAMBIT and I-DEAS. This helps to maximize productivity. Up-to-date pre-processors also

give the user access to libraries of material properties for common fluids and a facility to invoke special physical and chemical process models (e.g. turbulence models, radiative heat transfer, combustion models) alongside the main fluid flow equations.

3.5.2.2 Solver:

Numerical methods form the basis of the solver. They perform the following steps:

- Approximation of the unknown flow variables by means of simple functions
- Discretisation by substitution of the approximation into the governing flow equations and subsequent mathematical manipulations
- Solution of the algebraic equations

There are four distinct streams of numerical solution techniques:

(i) Finite difference method,

(ii) Finite element method,

(iii) Spectral methods, and

(iv) Finite Volume Method.

The main difference between these methods is the way in which the flow variables are approximated and with the discretisation process.

3.5.2.2.1 Finite Difference Method: This method was introduced by Euler in the 18th century (Douglas, et al). It is much like a differential quotient, except that it uses finite quantities instead of infinitesimal ones. The unknowns of the flow problem are described by point samples at the node points of the grid. This means each node has one unknown and one algebraic equation which is a

relation between the variable values at that node and those at some of the neighboring nodes.

3.5.2.2.2 Finite Element Method: This theory was at first developed for stress analysis of Structures. Simple piecewise functions (e.g. linear or quadratic), valid on elements, are used to describe the local variations of the unknown flow variables. The governing equation is satisfied by exact solution of the unknown variable. A residual is defined to measure the errors if the piecewise approximating functions for the unknown variable are substituted into the equation. Next the residuals (and hence the errors) are then minimized by multiplying them by a set of weighting functions and integrating. As a result a set of algebraic equations for the unknown coefficients of the approximating functions are obtained.

3.5.2.2.3 Spectral Methods: This method was originally developed for global weather Modeling. It involves the approximation of the unknowns by truncated Fourier series or series of Chebyshev polynomials. In this case the approximations are valid throughout the entire computational domain. The constraint that leads to the algebraic equations for the coefficients of the Fourier or Chebyshev series is provided by a weighted residual concept similar to the finite element method or by making the approximate function coincide with the exact solution at a number of grid points.

3.5.2.2.4 ***Finite Volume Method:*** The finite volume method was at first developed as a special finite difference Formulation. It is a well-established and thoroughly validated general purpose CFD technique and it is central to most of the commercially available CFD codes: ANSYS, FLUENT, PHOENICS, FLOW3D, FEM and STAR-CD [18]. The numerical algorithm consists of the following steps:

- Formal integration of the governing equations of fluid flow over all the control volumes of the solution domain.

- Discretisation involves the substitution of a variety of finite-difference-type approximations for the terms in the integrated equation representing flow process such as convection, diffusion and sources. This converts the equations into a system of algebraic equations.

- Solution of the algebraic equations by iteration.

The control volume (CV) integration, distinguishes the finite volume method from all other CFD techniques. The resulting statements express the conservation of relevant properties for each finite size cell. This clear relationship between the numerical algorithm and the underlying physical conservation principle forms one of the main attractions of the finite volume method and makes its concepts much simpler to understand by engineers than the finite element and spectral methods. The conservation of a general flow variable e.g. a velocity component, within a finite control volume can be expressed as a balance between the various processes tending to increase or decrease it.

CFD Codes contain discretisation techniques suitable for the treatment of the key transport phenomena, convection (transport due to fluid flow) and diffusion (transport due to variations of the variable from point to point) as well as for the source terms and the rate of change with respect to time. The underlying physical phenomena are complex and non-linear so an iterative solution approach is required. The most popular solution procedures are the TDMA line-by-line solver of the algebraic equations and the SIMPLE algorithm to ensure correct linkage between pressure and velocity [18].

3.5.2.3 Post-processor:

As in pre-processing a huge resource has been devoted to the development post processing techniques and display. Owing to the increased popularity of engineering workstations, many of which have outstanding graphics capabilities, the leading CFD packages are now equipped with versatile data visualization tools. These include:

- Domain geometry and grid display
- Vector plots
- Line and shaded contour plots
- 2D and 3D surface plots
- Particle tracking
- View manipulation (translation, rotation, scaling etc)
- Color postscript output

Currently animation facilities for dynamic result display have been included in many CFD packages. In addition to graphics all codes produce trusty alphanumeric output and have data export facilities. As in many other branches of CAE the graphics output capabilities of CFD codes have revolutionized the communication of ideas to the non-specialist and specialist alike.

3.5.3 Problem Solving With CFD:

The results generated by a CFD code are at best as good as the physics (and

Chemistry) embedded in it and at worst as good as its operator. Prior to setting up and running a CFD simulation there is a stage of identification and formulation of the flow problem in terms of the physical and chemical phenomena that need to be considered as discussed earlier. Typical decisions that might be needed are whether to model a problem in two or three dimensions, to exclude the effects of ambient temperature or pressure variations

on the density of an air flow, to choose to solve the turbulent flow equations or to neglect the effects of small air bubbles dissolved in tap water. To make the right choices requires good modeling skills, because in all but the simplest problems assumptions need to be made to reduce the complexity to a manageable level whilst preserving the salient features of the problem in hand [18] . It is appropriate that the simplifications introduced partly govern the quality of the information generated by CFD, so the user must continually stay aware of all the assumptions which have been made.

Chapter Four

Methodology

4.1 Introduction:

This chapter gives the flow description in axial flow turbine and the governing questions of motion for incompressible fluid, and turbulence model, also gives the geometry modelling and creation of mesh and setup of the problem such as (Physics, Fluid properties, Boundary condition…ect, and Solver parameters), and post-processing using CFD code ,Ansys CFX 10.0.

4.2 Basic flow description:

The flow in axial flow turbine (Kaplan) is very complex including several flow phenomena, such as turbulence, separation, swirling flow and unsteadiness flow. Advanced fluid flows are described by the continuity and momentum equations, which can generally not be solved analytically. Therefore the numerical procedure in CFD is of highest importance. In CFD the governing equations are discretized and solved for small domains, control volumes (CV). This provides numerical results of the predicted flow field in discrete locations, nodal points, in both space and time. In most CFD the governing equations are usually discretized by a Finite Volume Method (FVM) approach [19].

4.3 Governing Equations:

A flow can be considered incompressible if the density is constant in time and space. From the principle of mass conservation, the continuity equation for incompressible flow can be derived.

$$\frac{\partial U_j}{\partial x_j} = 0 \quad \text{..... (4.1)}$$

The incompressible Navier-Stokes can be expressed as:

$$\left(\frac{\partial}{\partial t}+\frac{\partial u_j}{\partial x_j}\right)u_i=-\frac{1}{\rho}\frac{\partial}{\partial x_i}p+v\frac{\partial}{\partial x_j}\frac{\partial}{\partial x_j}u_i \quad \text{..... (4.2)}$$

Where i = j = 1, 2, 3…ect.

4.4 Turbulence Modelling:

Turbulence consists of fluctuations in the flow field in time and space. It is a complex process, mainly because it is three dimensional, unsteady and consists of many scales. It can have a significant effect on the characteristics of the flow. Turbulence occurs when the inertia forces in the fluid become significant compared to viscous forces, and is thus characterised by a high Reynolds Number.

In principle, the Navier-Stokes equations describe both laminar and turbulent flows without the need for additional information. However, turbulent flows at realistic Reynolds numbers span a large range of turbulent length and time scales and would generally involve length scales much smaller than the smallest finite volume mesh which can be practically used in a numerical analysis. The Direct Numerical Simulation (DNS) of these flows would require computing power which is many orders of magnitude higher than available in the foreseeable future [20].

Instead the effects of turbulence are dealt with by usage of turbulence models; hence a large amount of CFD research is devoted to the development of such models. In this work Shear Stress Transport (SST) turbulence models will be applied, turbulence models are specifically designed to account for the effects of turbulence without the need of prohibitively fine grid and Direct Numerical Simulation (DNS). And most of them are based on statistics turbulence model, as described below.

4.4.1 Statistical Turbulence Models:

Considering time scales much larger than the time scales of the turbulent fluctuations, the turbulent flow can be said to exhibit average characteristics, with

an additional time-varying, fluctuating component. Statistical turbulence models uses this characteristic to modify the Navier-Stokes equations by introducing an averaged and a fluctuating quantity to produce the Reynolds Averaged Navier-Stokes (RANS) equations.

$$\partial_i U_i + U_j \partial_j U_i = -\frac{1}{\rho}\partial_i P + \nu \nabla^2 U_i - \partial_j \overline{u_j u_i} \quad \text{..... (4.3)}$$

$$\partial_i U_i = 0 \quad \text{..... (4.4)}$$

Where U_i is mean velocity, ρ is the fluid (water) density, P is the pressure, ν is the viscosity, $u_j u_i$ is the Reynolds stresses and u_i is the velocity fluctuation. For a more elaborate derivation of these equations please read [21]. These equations represent the mean flow characteristics, while the turbulent fluctuations (all scales) are modelled via the Reynolds stresses without the high resolution requirements.

Turbulence models based on the RANS equations are known as Statistical Turbulence Models due to the statistical averaging procedure employed to obtain the equations.

Simulation of the RANS equations greatly reduces the computational effort compared to a Direct Numerical Simulation and is generally adopted for practical engineering calculations. However, the averaging procedure introduces additional unknown terms containing products of the fluctuating quantities, which act like additional stresses in the fluid. These terms, called (turbulent) or (Reynolds) stresses, are difficult to determine directly and so become further unknowns.

The Reynolds (turbulent) stresses need to be modelled in order to achieve closure. Closure implies that there are a sufficient number of equations for all the unknowns, including the Reynolds-Stress tensor resulting from the averaging procedure. The equations used to close the system define the type of turbulence model.

4.4.2 Wall-functions:

Near a no-slip wall, there are strong gradients for the dependent variables. In addition, viscous effects on the transport processes are large. The representation of these processes within a numerical simulation raises a couple problems, such as how to account for viscous effects at the wall and how to resolve the rapid variation of flow variables which occurs within the boundary layer region.

Experiments and mathematical 2D analysis has shown that the near-wall region can be subdivided into two layers. The innermost layer, the so-called "viscous sublayer'' where the flow is almost laminar and where the (molecular) viscosity plays a dominant role in momentum and heat transfer. Further away from the wall, the "logarithmic layer," take place where turbulence dominates the mixing process. Finally, there is a region between the viscous sublayer and the logarithmic layer called the "buffer layer," where the effects of molecular viscosity and turbulence are of equal importance. The figure below illustrates these subdivisions of the near-wall region.

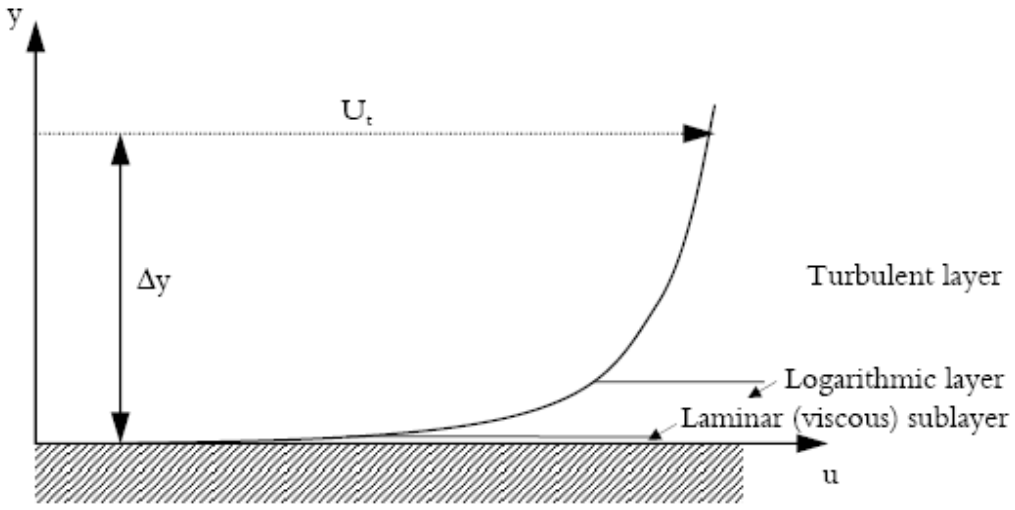

Fig (4.1): The subdivisions of the near-wall region

Assuming that the logarithmic profile reasonably approximation of the velocity

distribution near the wall, the fluid shear stress can be numerically compute as a function of the velocity at a given distance from the wall. This is known as a 'wall function' and the logarithmic nature gives rise to the well known log law of wall.

There are two approaches that are commonly used to model turbulence flow in the near-wall region:

- The Wall Function method where empirical formulas are used that imposes suitable conditions near to the wall without resolving the boundary layer, thus saving computational resources. The major advantages of the wall-function approach are that the high gradient shear layers near walls can be modelled with relatively coarse grids, yielding substantial savings in CPU time and storage. It also avoids the need to account for viscous effects in the turbulence model.

- The Low-Reynolds-Number method which resolves the details of the boundary layer profile by using very small grid length scales in the direction normal to the wall (very thin inflation layers). The low-Re method does note refer to the device Reynolds number, but to the turbulent Reynolds number, which is low in the viscous sublayer. This method can therefore be used even in simulations with very high device Reynolds numbers, as long as the viscous sublayer has been resolved.

The low-Re approach requires a very fine gird in the near-wall zone and correspondingly large number of nodes. Computer-storage and runtime requirements are higher than those of the wall-function approach and care must be taken to ensure good numerical resolution in the near-wall region to capture the rapid variation in variables. To reduce the resolution requirements, an automatic wall treatment was developed by CFX, which allows a gradual switch between wall functions and low-Reynolds number grids, without a loss in accuracy.

4.4.3 The Shear Stress Transport (SST) model:

One of the main problems in turbulence modelling is the accurate prediction of flow separation from a smooth surface. Ordinary two-equation turbulence models as the standard k-ε model often fail to predict the onset and the amount of flow separation under adverse pressure gradient conditions. This is an important phenomenon in many technical applications, particularly for airplane aerodynamics since the stall characteristics of a plane are controlled by the flow separation from the wing. For this reason, the aerodynamic community has developed a number of advanced turbulence models for this application. In general, turbulence models based on the ε-equation predicts the onset of separation too late and under-predict the amount of separation later on. This is problematic, as this behavior gives an overly optimistic performance characteristic for an airfoil. The prediction is therefore not on the conservative side from an engineering point of view. The models developed to solve this problem, as the k-ω model has shown a significantly more accurate prediction of separation in a number of test cases and in industrial applications. Separation prediction is important in many technical applications both for internal and external flows.

Currently, on of the most prominent two-equation models in this area is the Shear-Stress-Transport model (SST) by Menter [22]. The idea behind the SST-model is to combine the best elements of the k-ε and the k-ω model with the help of a blending factor. The blending factor decides which of the two turbulence models that is the most prominent. It activates the k-ω model in the near-wall region and the k-ε model for the rest of the flow. The transition from the k-ω to the k-ε formulation takes place in the logarithmic layer. By this approach, the attractive near-wall performance of the k-ω model can be utilized

without the potential errors resulting from the free stream sensitivity of that model.

The model is based on the Bradshaw's assumption that the principal shear-stress is proportional to the turbulent kinetic energy, which is introduced into the definition of the eddy-viscosity.

A short derivation of the model is as follows, for more details [22]:

The original k-ω formulation is given by:

$$\frac{\partial(\rho k)}{\partial t} + \nabla.(\rho U k) = \nabla.\left[\left(\mu + \frac{\mu_t}{\sigma_{k1}}\right)\nabla k\right] + P_k - \beta'\rho k\omega \quad \text{(4.5)}$$

$$\frac{\partial(\rho \omega)}{\partial t} + \nabla.(\rho U \omega) = \nabla.\left[\left(\mu + \frac{\mu_t}{\sigma_{\omega 1}}\right)\nabla \omega\right] + \alpha_1 \frac{\omega}{k} P_k - \beta_1 \rho \omega^2 \quad \text{(4.6)}$$

And the transformed standard k-ε formulation (to a k-ω formulation) is given by:

$$\frac{\partial(\rho k)}{\partial t} + \nabla.(\rho U k) = \nabla.\left[\left(\mu + \frac{\mu_t}{\sigma_{k2}}\right)\nabla k\right] + P_k - \beta'\rho k\omega \quad \text{(4.7)}$$

$$\frac{\partial(\rho \omega)}{\partial t} + \nabla.(\rho U \omega) = \nabla.\left[\left(\mu + \frac{\mu_t}{\sigma_{\omega 2}}\right)\nabla \omega\right] + 2\rho\frac{1}{\sigma_{\omega 2}\omega}\nabla k.\nabla\omega + \alpha_2 \frac{\omega}{k} P_k - \beta_2 \rho \omega^2 \quad \text{(4.8)}$$

Now if equation (4.5) and (4.6) are multiplied by a blending factor F_1 and equation (4.7) and (4.8) are multiplied by its reverse (1-F_1), the SST model is obtained by adding each set of equations together, i.e.:

$$\frac{\partial(\rho k)}{\partial t} + \nabla.(\rho U k) = \nabla.\left[\left(\mu + \frac{\mu_t}{\sigma_{k3}}\right)\nabla k\right] + P_k - \beta'\rho k\omega \quad \text{(4.9)}$$

$$\frac{\partial(\rho \omega)}{\partial t} + \nabla.(\rho U \omega) = \nabla.\left[\left(\mu + \frac{\mu_t}{\sigma_{\omega 3}}\right)\nabla \omega\right] + (1 - F_1)2\rho\frac{1}{\sigma_{\omega 2}\omega}\nabla k.\nabla\omega + \alpha_3 \frac{\omega}{k} P_k - \beta_3 \rho \omega^2 \quad \text{(4.10)}$$

The blending factor $F1$ in equation (4.9) and (4.10) is defined as:

$$F_1 = tanh(arg_1{}^4) \quad \text{(4.11)}$$

Where arg_1 in next turn is defined as:

$$arg_1 = min\left[max\left(\frac{\sqrt{k}}{\beta' \omega y}; \frac{500\nu}{y^2 \omega}\right); \frac{4\rho k}{CD_{k\omega}\sigma_{\omega 2} y^2}\right] \quad \text{.....(4.12)}$$

Where y is the distance to the next surface and $CD_{k\omega}$ is the cross-diffusion term of equation (4.12):

$$CD_{k\omega} = max\left(2\rho \frac{1}{\sigma_{\omega 2}\omega} \nabla k . \nabla \omega; 1.0 * 10^{-10}\right) \quad \text{.....(4.13)}$$

F_2 is a second blending factor defined as:

$$F_2 = \tanh(arg_2{}^2) \quad \text{..... (4.14)}$$

Where arg_2 in next turn is defined as:

$$arg_2 = max\left(\frac{2\sqrt{k}}{\beta' \omega y}; \frac{500\nu}{y^2 \omega}\right) \quad \text{..... (4.15)}$$

The model constants in the above equations are given by the relation:

$$\phi = F_1 \phi_1 + (1 - F_1)\phi_2 \quad \text{.....(4.16)}$$

Where $\emptyset_1$represent any constant in the k-ω model (σ_{k1},…), $\emptyset_2$ any constant in the transformed k-ε model (σ_{k2} ,…) and $\emptyset$ the corresponding constant of the SST model(σ_k,…) the following sets of constant are standard values:

Set1(k-ω):

$$\sigma_{k1} = 2, \sigma_{\omega 1} = 2, \beta_1 = 0.075, \alpha_1 = 0.55, \beta' = 0.09, k = 0.41$$

Set 2 (Standard k-ε):

$$\sigma_{k2} = 1.0 \quad , \quad \sigma_{\omega 2} = 0.856 \quad , \quad \beta_2 = 0.0828 \quad , \quad \alpha_2 = 0.44, \beta' = 0.09 \, ,$$
$$k = 0.41$$

4.5 Case study:

The Kaplan turbine has the following data in the table below is used as case study of this research and different operation conditions are used.

Table (4.1): The data of the Kaplan turbine.

Number of blades	6
Rotational speed	137 r.p.m
Outer diameter (Shroud)	6m
Inner diameter (Hub)	3m
Available head	40 m
Mass flow rate	116m^3/s

4.6 Computational Approach:

This section describes the numerical considerations. The set-up of boundary condition and grid generation are also discussed. The commercial CFD code Ansys workbench, CFX 10.0 is used to solve the flow in the runner blades, with assumption of steady, incompressible and turbulent water flow.

The turbulence in the runner is modeled with SST turbulence model using the standard wall function.

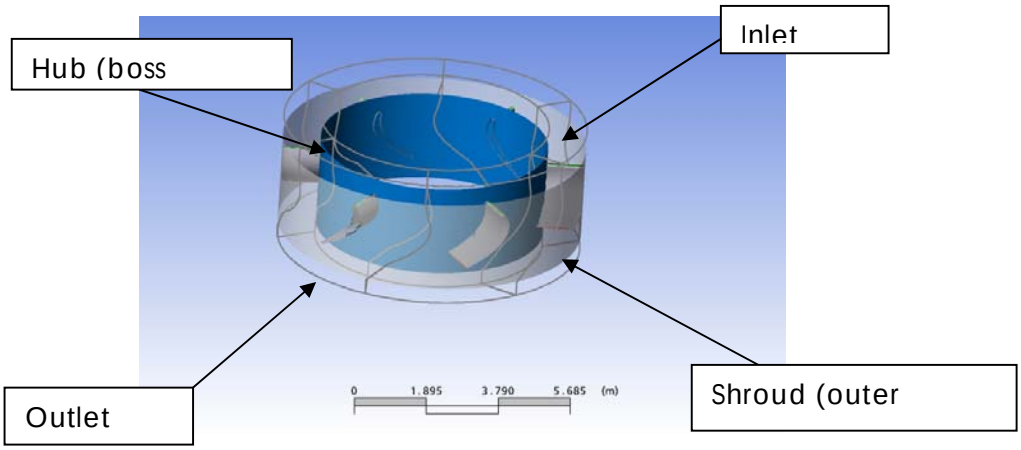

Fig (4.2): Six blades geometry

4.6.1 Computational domain:

The computational domain is build and modified with the commercial Blade Generator offered in Ansys workbench software. Often it starts as a simple axial flow water turbine (Kaplan) of six blades. The blade data and all other dimension admitted to the package such as chamber, thickness, location of maximum thickness form leading edge and angles See Appendix (A). An exported to Turbo Grid software offered in Ansys to generate the 3D meshing Figures from (4.3) to (4.6) represents the Computation domain of this work.

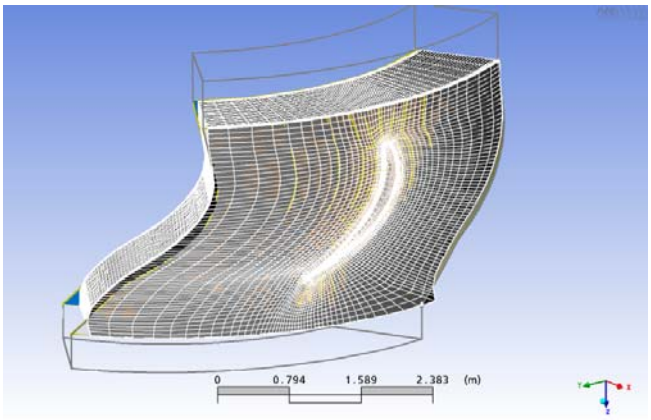

Fig (4.3): Computation domain single blade meshing.

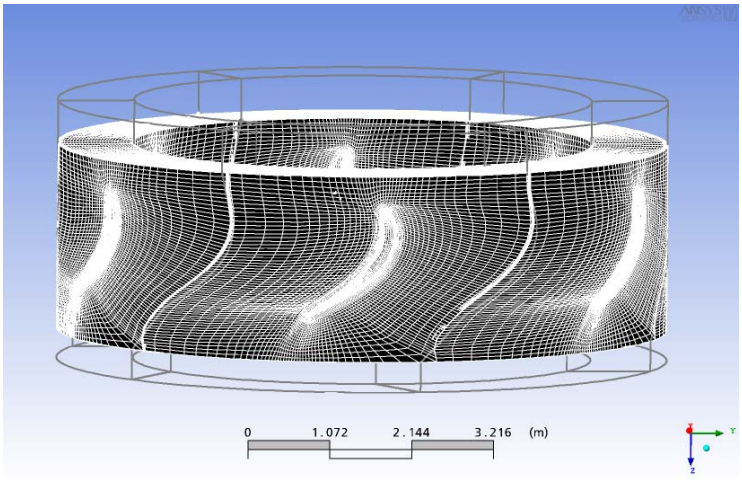

Fig (4.4): Computation domain of six blades meshing

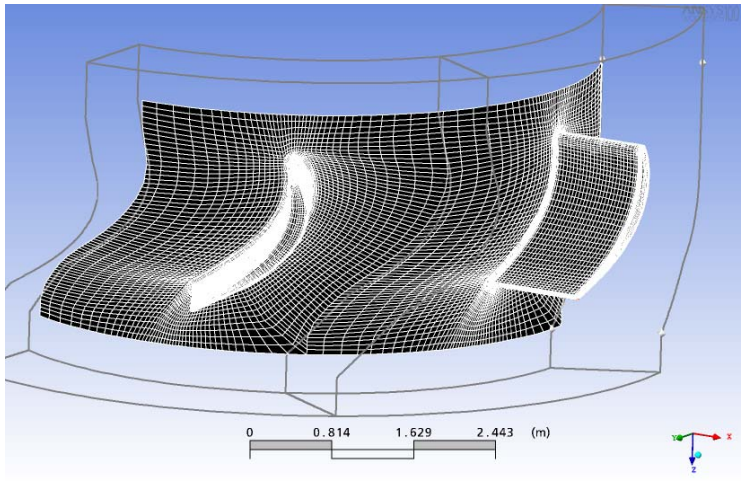

Fig (4.5): Shows tow blades meshing hub side

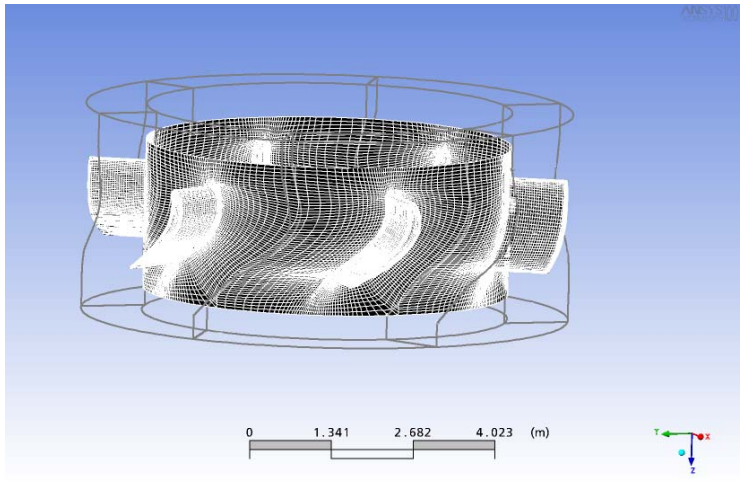

Fig (4.6): shows six blades meshing hub side

4.6.2 Boundary conditions:

The boundary conditions set in the CFD simulation are the same as those from the operational mode of the case study of this work, collected from hydropower plant reference [23]. This mode represents the point with highest efficiency on the propeller curve, i.e. optimum operation condition. At the inlet, the boundary condition is given by mass flow rate, and static pressure is set at outlet boundary condition, and the wall is set as no-slip for each wall.

4.6.3 Numerical procedure:

The CFD code, Ansys workbench, considers all meshes as hybrid and discretization is done with a cell centered finite volume method.

Since the flow in the runner is assumed to be turbulent, and incompressible, the Reynolds–Averaged Navier-stokes equations are used. In order to solve these governing equations in Ansys workbench, the CFX10.0 solver has been utilized in this study. The SST model was used to model the Reynolds stress terms and to close the governing equations.

The computational grids consist of unstructured hexahedral elements (CVs) and are generated in Turbo Grid software offered in Ansys workbench. The main reason for the choice of hexahedral grid is to get a higher accuracy and speed of the calculation. The following table (4.2) shows the number nodes in the whole domain, and mesh definition in Fig (4.7).

Table (4.2): The different number of nodes:

Parameter	Case one	Case Two	Case Three
Number of Nodes	225672	255560	352696
Number of Elements	212252	240924	334108
Hexahedra	212252	240924	334108

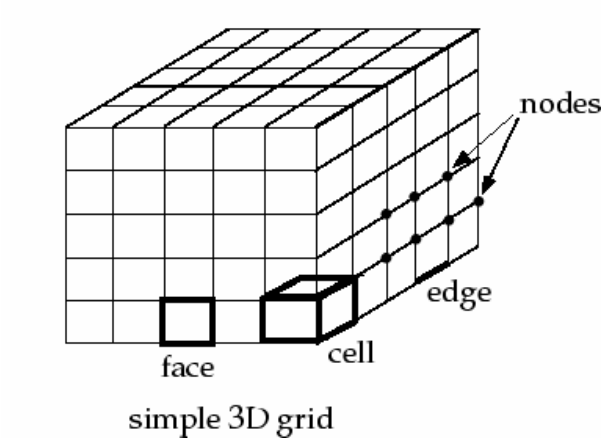

Fig (4.7): Shows the mesh data definition.

Note, that the geometry modelled is only a part of whole hydropower system, since the amount of required elements to model the whole plant would be enormous

.

Chapter Five

Results and discussion

5.1 Results and discussion:

The CFD simulations are assumed converged when all the residuals are less than10^{-7}, which is sufficient for most engineering problems. The velocity at points at the inlet, the centre and at the outlet is monitored and when there is no change in the results are considered converged. The distinct rise in the residual plot is due to the change in the differencing schemes.

The convergence of the SST turbulence model in this study is assumed converged when the residuals plots drop to 10^{-7} and the difference of mass flow in and mass flow out is very small compared to mass flow in. Fig (5.1) shows the residual plot of momentum and mass for three cases.

From the residual of mass and momentum for three cases, (A) the case of $255*10^3$ nodes is accepted because the residual plots is constant for long iteration and no change is the values of velocities components, (B) the case of $225*10^3$ nodes the residual plots is less than the residual target, (C) the case of $352*10^3$ nodes there is fluctuation in the value of v-component due to computer capabilities and grid quality, all the following results are taken for the case two of $255*10^3$ nodes.

Fig(5.2) show clearly the static pressure distribution between two successive blades of the turbine. Here,(it is very clear the high pressure excerted on the pressure side of blade and low pressure in blade suction side, this valid for all blades and according to the theorm of terbomachinery the pressure side is higher than suction side of the blade.

Results confirm that the pressure drops gradually form the inlet to outlet due to the extraction of fluid energy by the turbine runner.

Fig(5.3) show the pressure variation from inlet to outlet this means that the pressure decreased from inlet to leading edge and then increased at the leadig edge after that decreased gradually along the blade until reach the tailing edge then increased to leaves with atomspheric pressure.

Fig(5.4) show the variation velocity component from inlet to outlet along the streamwise,the velocity component U in x-direction starting from small value near to zero and incearesed gradually along the streamwise(radial direction of blade), the velocity component V in Y- direction is very small startnig from negative value and increased gradually along the streamwise until reach the vlaue less than zero this in the direction of blade span,the velocity component W in Z-direction is semi constant along the streamwise this in the direction of rotational but the total velocity decreased from inlet to outlet due to rotation, swirling and vortex occur.

Fig(5.5) show the performance curves of the of blade under different operation condition, this indicate that the efficiency of the turbine balde increased with increasing of N rpm until reach maximum poit and then decreased gradully (parabolic shap) this valid only for N from 120 to 150 rpm out of this range the efficiency is varies.The power also increased with the increase of N rpm to maximum also this is valid for N from 120 to 160 rpm.

Fig (5.6) show the streamlines at hub,shroud and blade, (A) at the hub this indicate that, there is vrotex occur at the suction side of the blade near the tailing edge where the low pressure region.(B) at the shroud this means that the water flow path in the tip clearance. At (C) the streamlines in pressure surface of blade indicate the path of water flow over pressure side, (D) the streamlines at suction surface of the blade where the vortexes occur and it's very clear at velocity vector.

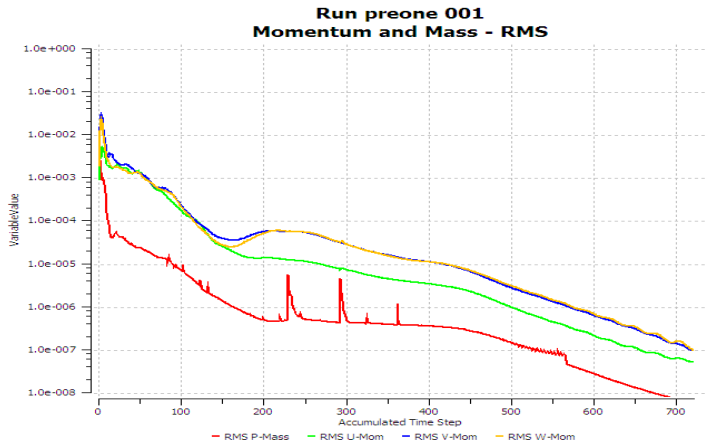

(A)

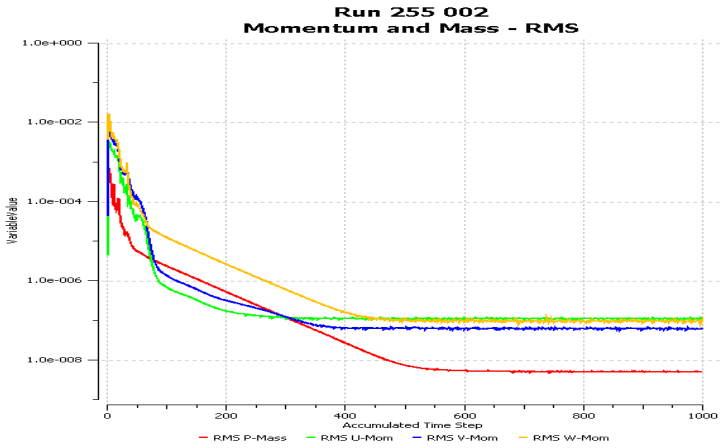

(B)

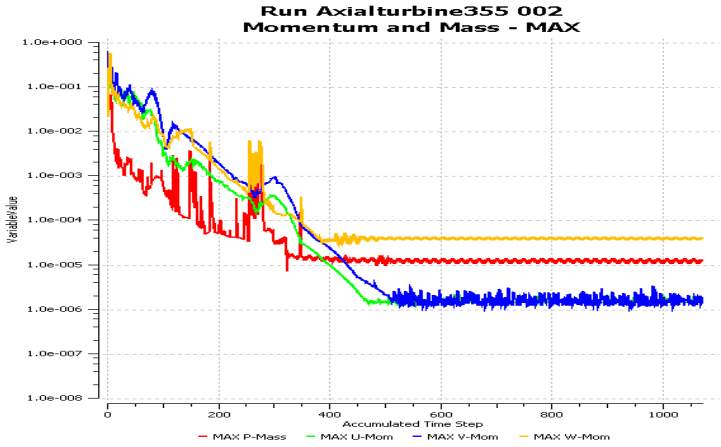

(C)

Fig (5.1) Residual plots for (A) $225*10^3$ nodes (B) $255*10^3$ nodes (C) $^{352}*10^3$ nodes.

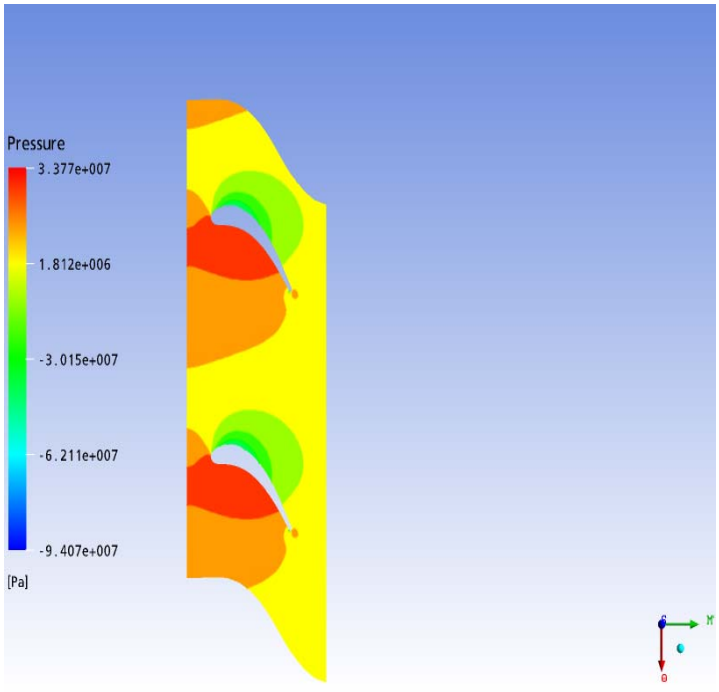

(A)

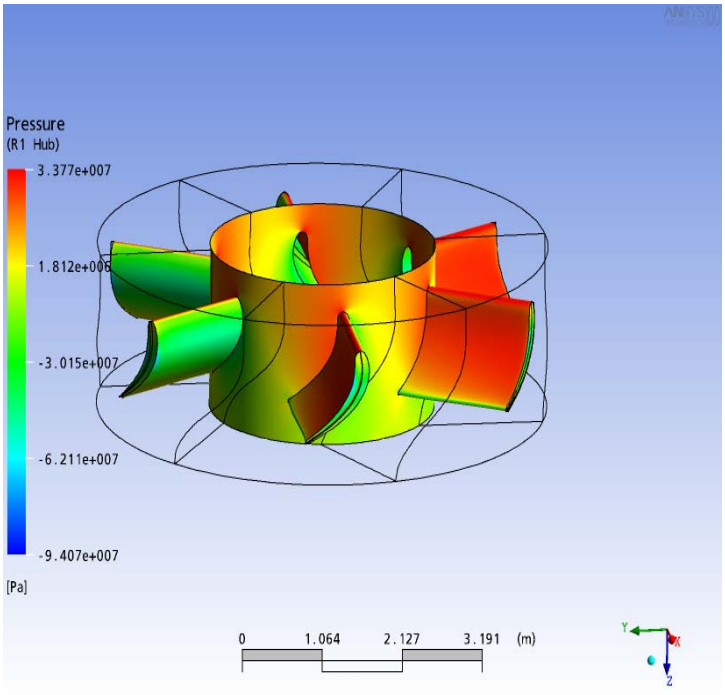

(B)

Fig (5.2) Static pressure distribution on (A) plane at mean radius

(B) Blades.

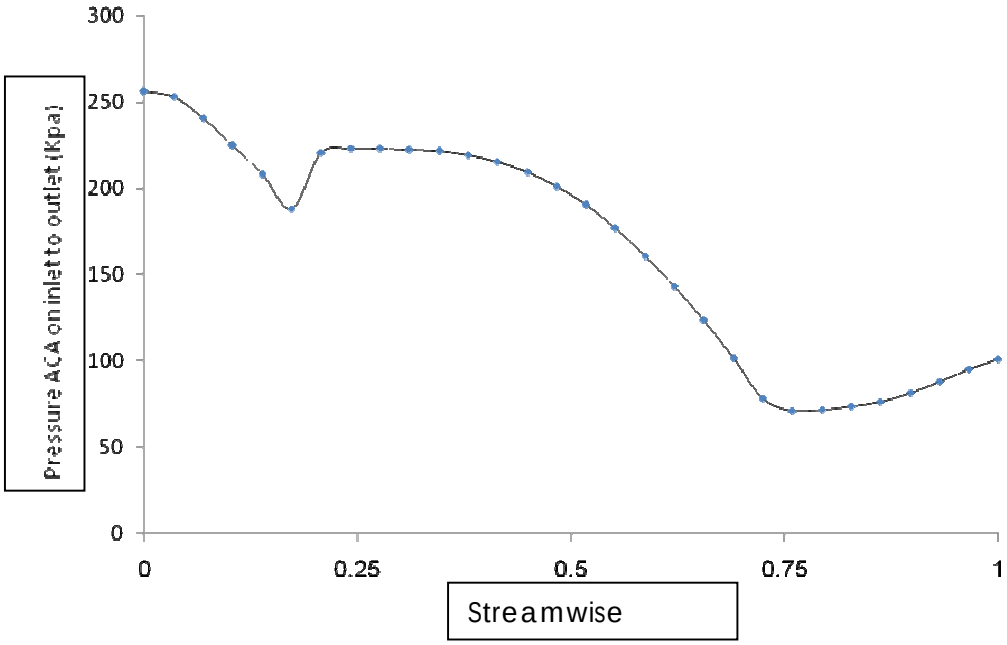

Fig (5.3) Variation of Pressure ACA form inlet to outlet

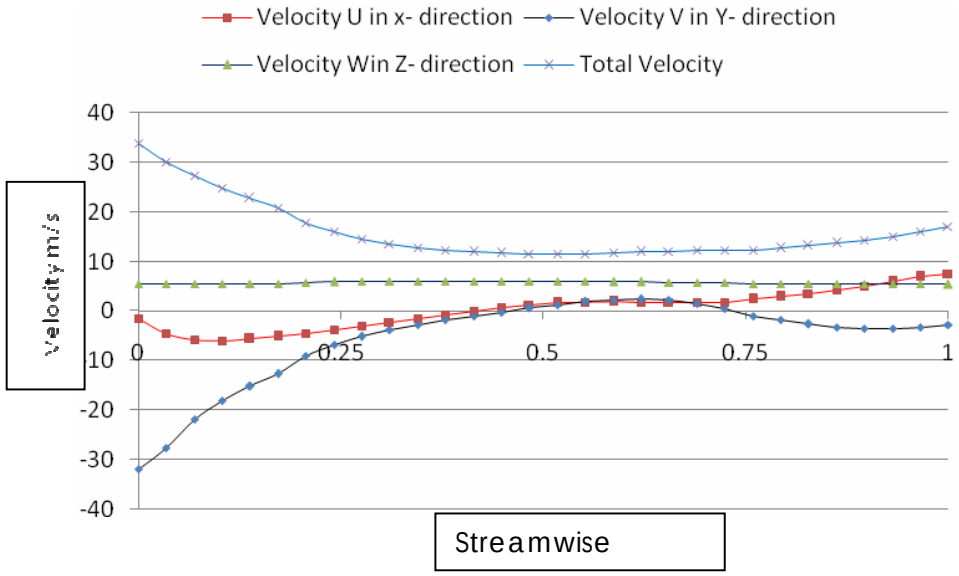

Fig (5.4) Variation of velocities from inlet to outlet

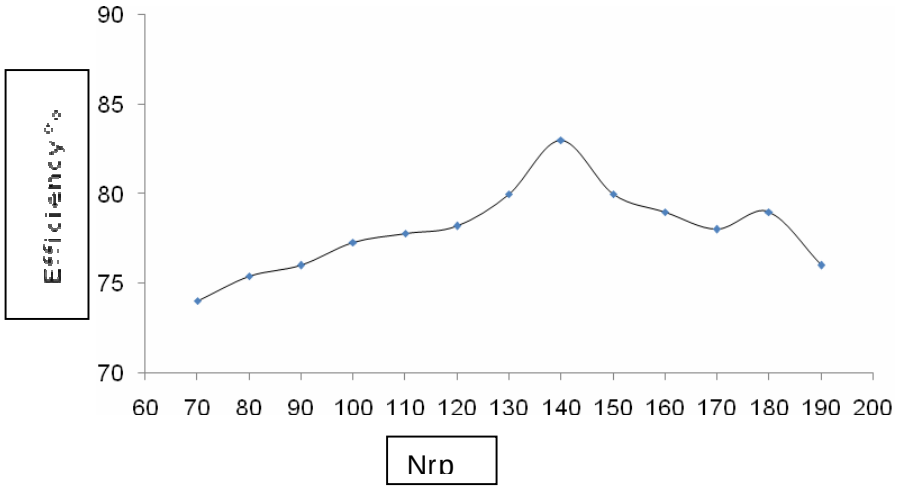

(A)

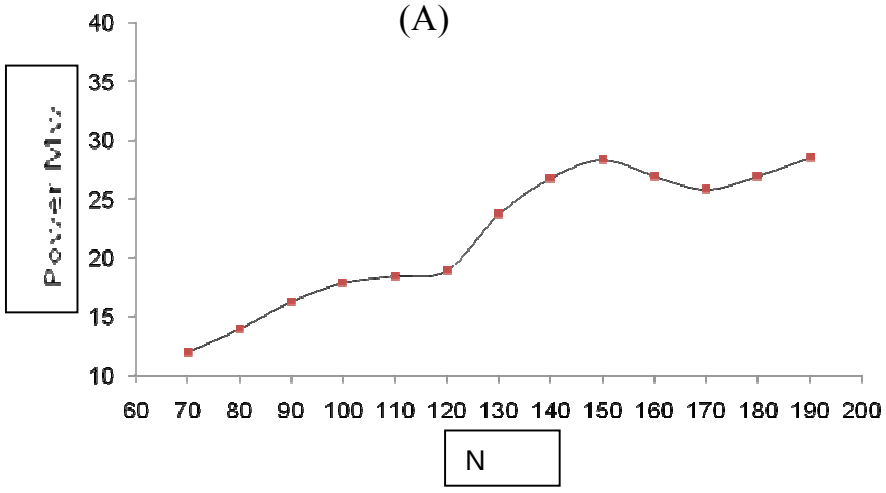

(B)

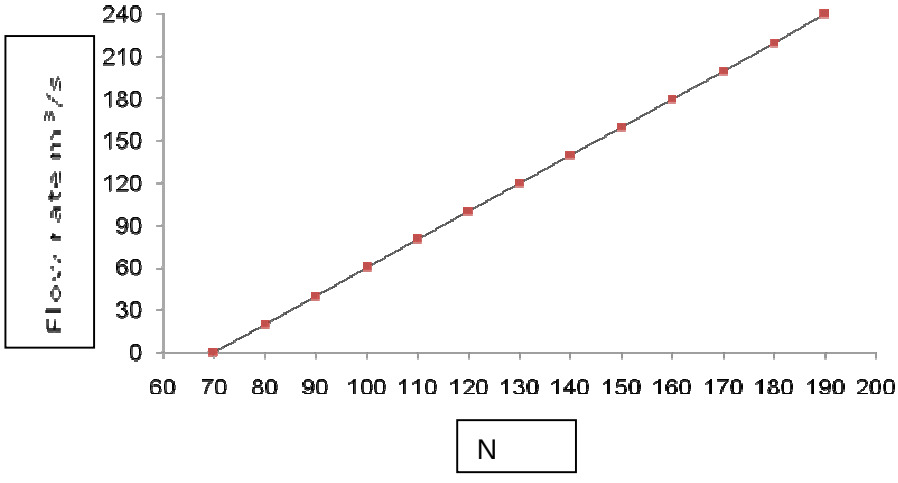

(C)

Fig (5.5) Performance Curves (A) Efficiency vs Rotational Speed(B) Power vs Rotational Speed (C) Flow rate vs Rotational Speed.

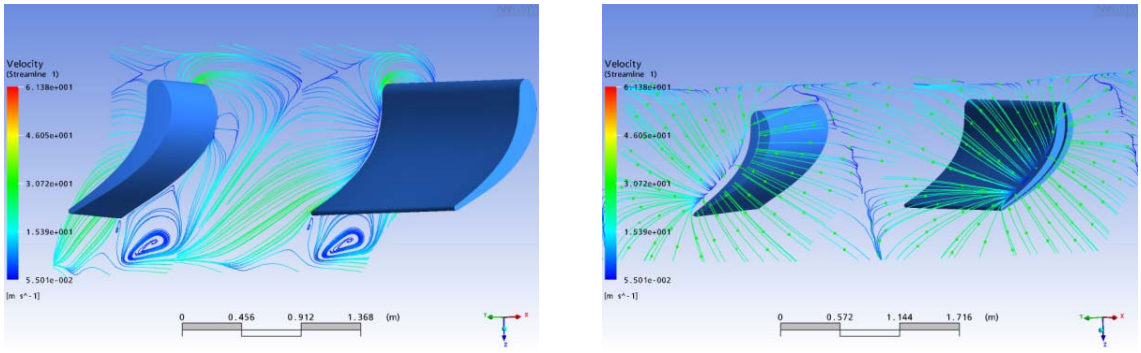

(A) (B)

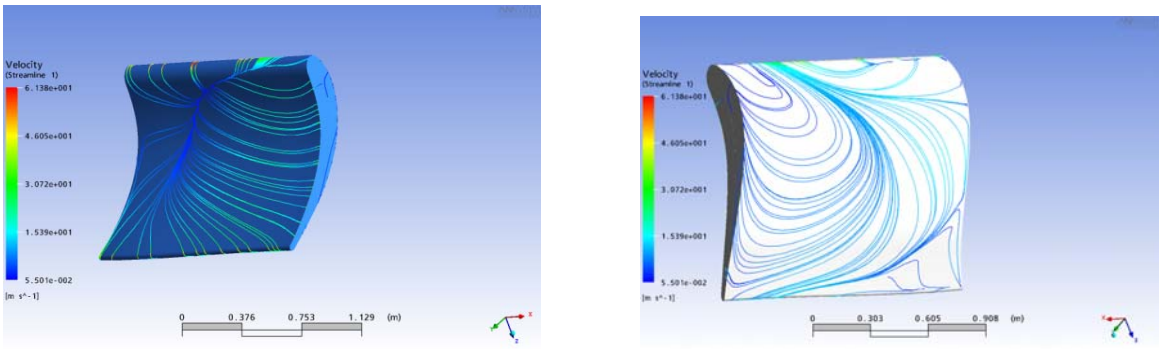

(C) (D)

Fig (5.6) streamlines (A) on Hub surface (B) on Shroud plane (C) On Blade-pressure surface (D) on Blade-suction surface.

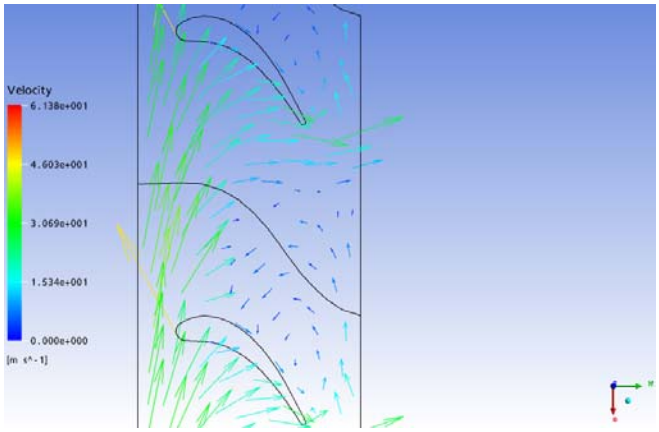

Fig (5.7) Velocity vector on plane at mean radius

Chapter Six

Conclusion and Recommendations

6.1 Conclusion:

The thesis reports simulation of the turbulent flow of water in axial turbine. The turbine blade runner is designed by "Blade modeler package" available in ANSYS workbench 10. The simulations are done by using CFX.10 to show the performance of the blade under different operation conditions. The method of simulation is principally numerical. The results indicate that:

1- The power increased with the increase of N rpm.

2- The variation of the pressure from hub to shroud increased gradually.

3- The pressure drop from inlet to outlet according to turbomachinery theorem.

4- The streamlines shows some vortexes occur at the suction side of blade near to tailing edge.

The computations of the flow in water turbines require careful attention to the grid quality, to their density, distribution and discretization scheme in order to capture the details of the flow.

Computational methods can be used to understand the details of the flow field in Kaplan turbine runner. This has shown itself difficult to understand by experimental work. Then it’s a best practice to introduce CFD package to know more details about flow field

The ANSYS workbench10.0 CFX code that was used in the present work produces accurate predictions of the flow in Kaplan turbine runner. The code is also used and validated in academic test cases as well as in other industrial

applications such as LES (Large Eddy Simulations) of the flow around vehicles and airfoils and of heat transfer in gas turbines.

6.2 Recommendations:

Finally and for future work I recommended the following points:

1- The simulation must be compared with the experimental work for the same geometry dimensions, for validating the results obtained.

2- The Analysis must be done for the Kaplan runner blades with stator blades to know more details a bout the flow field analysis.

3- Using another commercially available CFD codes: FLUENT, PHOENICS, FLOW3D, FEM and STAR-CD and to compare the results with the results of ANSYS workbench – CFX10.0.

References

1- Conference of, "*production of electricity in Arabic Countries",* Khartoum Sudan. 2004.

2- World Energy Council, "*Survey of Energy Resources*", Technical Report, Sep.2006.

3- Krivchenko G., "*Hydraulic Machines: Turbines and Pumps"*,2ed., Lewis, Boca Raton. 1994.

4- Finnemore E.J.; Franzini J.B., "*Fluid Mechanics with Engineering Applications"*, 10ed., McGraw-Hill Companies, Inc. 2002.

5- Kjølle A., "*Water Power Machines (in Norwegian)"*, University, Oslo, Norway 1980.

6- Wislicenus G. F.: "*Fluid Mechanics of Turbomachinery"*, Volume 1 and 2, Dover Publication, New York, USA, 1965.

7- Schilling R., "*A high-performance and low-cost propeller turbine for small hydro schemes",* June 2001.

8- Cook T. C.; Heck G. E.; Faulkner H.B.; and Jansen W., "*Development of a more fish tolerant turbine runner–Advanced hydropower turbine project*",. DOE. 1997.

9- Rudkin E., "*Performance assessment of diffuser augmented water turbine"*, Msc. Thesis, March. 1998.

10- Nilsson H.; and Davidson, L., *CALC-PVM:, "A parallel Simplec Multiblock solver for turbulent flow in complex domains"*, Dept. of Thermo and Fluid Dynamics, Chalmers University of Technology, Gothenburg,.1998.

11- Nilsson H.; Andersson U.; and Videhult S., "*Flow in the Spiral Cas*ing", Chalmers University of Technology, Sweden, September 2001

12- Vesco Djelic, "*Efficiency Scale-up in Refurbished low head Kaplan Turbine"*, August, .2000.

13- Gallus H.E; Zeschky J.; Hah C., "*End wall and unsteady flow phenomena in an axial turbine stage"*, June 1994.

14- Wiriya Chanakul, Tonsirojn Jangrugsagul., "*Computer Programming for Efficiency for water turbines calculation"*.1999.

15- John Wiley., "*Design optimization of axial flow hydraulic turbine runner"*,. June. 2002.

16- Rama S.R Gorla. & Aijaz A. Kahn., "*Turbomachinery Design and Theory"*, Marcel Dekker, New York,. 2003.

17- Tullis J.P., "*Hydraulics of pipelines – pumps, valves, cavitation, transients"*. John Wiley & Sons, Inc., New York. 1989.

18- Versteeg, H. K. & Malalasekera W.,*''An introduction to computational fluid dynamics: the finite volume method'',* Harlow: Longman.1995,

19- Ferzinger J.H., Peric, M., "*Computational Methods for Fluid Dynamics*", Springer-Verlag, Berlin, Heidelberg, 3rd edition, 1999.

20- CFX Ltd, '' *CFX Version 10.0 Manual*'', The Gemini Building, Harwell International Business Centre, Oxfordshire, United kingdom.2005.

21- Durbin P.A., Pettersson Reif B.A., "*Statistical Theory and Modelling for Turbulent Flow*'', John Wiley and Sons, New York, 2000.

22- Menter F.R., *"Zonal Two equation k-ω Turbulence Models for Aerodynamic Flows*'', AIAA Paper 93 2096, July 1993.

23- Rajput R.K., "*A text book of power plant engineering*", New Delhi,3rd,2005.

24- http://www.wikipedia.org.

25- http://www.hydropowerenergy.edu.

Appendix (A)

The Ang/Thk Report:

Meridional Image

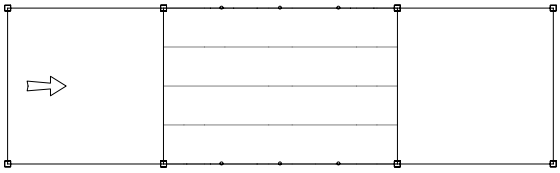

Meridional Curve Tab

Hub:Seg00:Bezier		Hub:Seg01:Bezier		Hub:Seg02:Bezier	
Axial (Z)	Degree (D)	Axial (Z)	Degree (D)	Axial (Z)	Degree (D)
0.5000	85.9437	1.5000	85.9437	3.0000	85.9437
1.5000	85.9437	1.8750	85.9437	4.0000	85.9437
		2.2500	85.9437		
		2.6250	85.9437		
		3.0000	85.9437		

Shroud:Seg00:Bezier		Shroud:Seg01:Bezier		Shroud:Seg02:Bezier	
Axial (Z)	Degree (D)	Axial (Z)	Degree (D)	Axial (Z)	Degree (D)
0.5000	143.2395	1.5000	143.2395	3.0000	143.2395
1.5000	143.2395	1.8750	143.2395	4.0000	143.2395
		2.2500	143.2395		
		2.6250	143.2395		
		3.0000	143.2395		

Inlet:Seg00:Bezier		Exit:Seg00:Bezier		LE:Seg00:Bezier	
Axial (Z)	Degree (D)	Axial (Z)	Degree (D)	Axial (Z)	Degree (D)
0.5000	85.9437	4.0000	85.9437	1.5000	85.9437
0.5000	143.2395	4.0000	143.2395	1.5000	143.2395

TE:Seg00:Bezier	
Axial (Z)	Degree (D)
3.0000	85.9437
3.0000	143.2395

Layer Definition Table

Layer Span: 0.0000:Seg00:Spline*		Layer Span: 0.0000:Seg01:Spline*		Layer Span: 0.0000:Seg02:Spline*	
Axial (Z)	**Degree (D)**	**Axial (Z)**	**Degree (D)**	**Axial (Z)**	**Degree (D)**
1.5000	85.9437	2.0250	85.9437	2.4750	85.9437
1.6312	85.9437	2.1750	85.9437	2.6063	85.9437
1.7625	85.9437	2.3250	85.9437	2.7375	85.9437
1.8937	85.9437	2.4750	85.9437	2.8688	85.9437
2.0250	85.9437			3.0000	85.9437

Layer Span: 0.2500:Seg00:Spline*		Layer Span: 0.2500:Seg01:Spline*		Layer Span: 0.2500:Seg02:Spline*	
Axial (Z)	**Degree (D)**	**Axial (Z)**	**Degree (D)**	**Axial (Z)**	**Degree (D)**
1.5000	100.2677	2.0250	100.2677	2.4750	100.2677
1.6313	100.2677	2.1750	100.2677	2.6063	100.2677
1.7625	100.2677	2.3250	100.2677	2.7375	100.2677
1.8937	100.2677	2.4750	100.2677	2.8688	100.2677
2.0250	100.2677			3.0000	100.2677

Layer Span: 0.5000:Seg00:Spline*		Layer Span: 0.5000:Seg01:Spline*		Layer Span: 0.5000:Seg02:Spline*	
Axial (Z)	**Degree (D)**	**Axial (Z)**	**Degree (D)**	**Axial (Z)**	**Degree (D)**
1.5000	114.5916	2.0250	114.5916	2.4750	114.5916
1.6312	114.5916	2.1750	114.5916	2.6062	114.5916
1.7625	114.5916	2.3250	114.5916	2.7375	114.5916
1.8937	114.5916	2.4750	114.5916	2.8688	114.5916
2.0250	114.5916			3.0000	114.5916

Layer Span: 0.7500:Seg00:Spline*		Layer Span: 0.7500:Seg01:Spline*		Layer Span: 0.7500:Seg02:Spline*	
Axial (Z)	**Degree (D)**	**Axial (Z)**	**Degree (D)**	**Axial (Z)**	**Degree (D)**
1.5000	128.9156	2.0250	128.9156	2.4750	128.9156
1.6312	128.9156	2.1750	128.9156	2.6062	128.9156
1.7625	128.9156	2.3250	128.9156	2.7375	128.9156
1.8938	128.9156	2.4750	128.9156	2.8687	128.9156
2.0250	128.9156			3.0000	128.9156

Layer Span: 1.0000:Seg00:Spline*		Layer Span: 1.0000:Seg01:Spline*		Layer Span: 1.0000:Seg02:Spline*	
Axial (Z)	**Degree (D)**	**Axial (Z)**	**Degree (D)**	**Axial (Z)**	**Degree (D)**
1.5000	143.2395	2.0250	143.2395	2.4750	143.2395
1.6312	143.2395	2.1750	143.2395	2.6063	143.2395
1.7625	143.2395	2.3250	143.2395	2.7375	143.2395
1.8937	143.2395	2.4750	143.2395	2.8688	143.2395
2.0250	143.2395			3.0000	143.2395

Normal Thickness Contour Plot

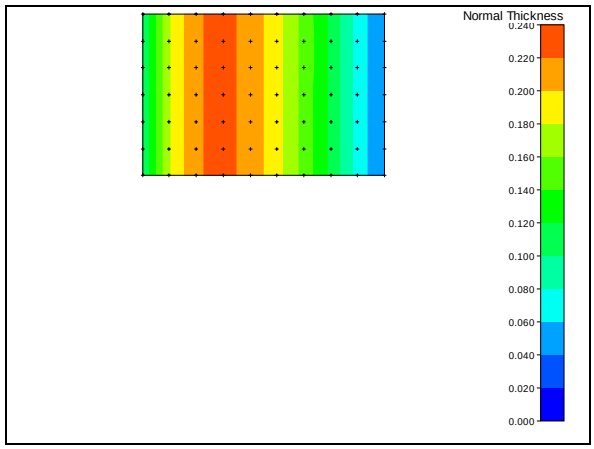

Beta (Blade Angle) Contour Plot

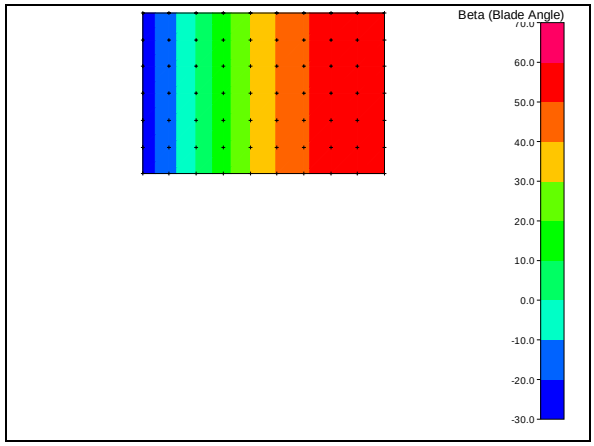

Theta (Blade Location) Contour Plot

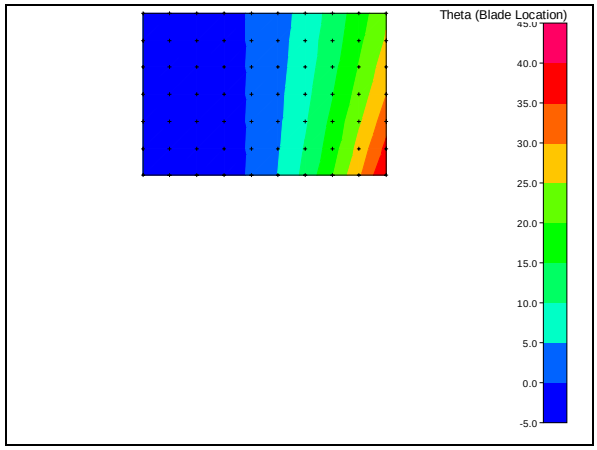

Blade Information Table ; System Parameters
Path 0: (0:0)

Parameter	Value
Corrected Throat Area	7.39551
Throat Surface Area	7.70268

Layer: Span: 0.0000
(coordinates shown in cylindrical coordinates <r,t,z>, with t in radians)

Parameter	Value
B2B Throat Length 0	0.824977
Segment 0: 0:(1.5,0.697899,2.97481) to 0:(1.5,1.09073,2.397420	0
Crv Throat Length 0	0.824869
LE Pitch	1.5708
TE Pitch (S)	1.5708
Centroid:Z	2.22521
Centroid:R	1.5
Centroid:T	6.5°
Centroid:Mp	0.483473
Centroid:M	0.725209
Airfoil Area	0.298544

Blade & Layer Parameters (using M vs T-Prime system)

Parameter	Value
3D Meanline Length	2.04172
Camber Length	2.04174
Cord Length (C)	1.83116
Meridional Length (M)	1.5
Stagger Angle	35.0°
Solidity (C/S)	1.16575
Pitch Cord Ratio (S/C)	0.857815

Bezier Parameters:
Standard Parameters:

Parameter	Value
Stagger Angle	35.0°
LE Theta Angle	0.0°
LE Beta Angle	-25.0°
TE Beta Angle	60.0°
LE Wedge Angle	15.0°
TE Wedge Angle	2.0°
LE Thickness	0.1
TE Thickness	0.0400036

Advanced Side1 Point Parameters:

Parameter	Value
First Point %M'	20.0
Last Point %M'	80.0

Linear Point %M'	30.0

Advanced Side2 Point Parameters:

Parameter	Value
First Point %M'	30.0
Last Point %M'	80.0
Linear Point %M'	0.0

Layer: Span: 0.2500
(coordinates shown in cylindrical coordinates <r,t,z>, with t in radians)

Parameter	Value
B2B Throat Length 0	1.01444
Segment 0: 0:(1.75,0.602614,2.97613) to 0:(1.75,1.04627,2.3231.0	1.0
Crv Throat Length 0	1.01425
LE Pitch	1.8326
TE Pitch (S)	1.8326
Centroid:Z	2.22578
Centroid:R	1.75
Centroid:T	5.7°
Centroid:Mp	0.41473
Centroid:M	0.725777
Airfoil Area	0.299196

Blade & Layer Parameters (using M vs T-Prime system)

Parameter	Value
3D Meanline Length	2.04718
Camber Length	2.04719
Cord Length (C)	1.83493
Meridional Length (M)	1.5
Stagger Angle	35.2°
Solidity (C/S)	1.00128
Pitch Cord Ratio (S/C)	0.998727

Layer: Span: 0.5000
(coordinates shown in cylindrical coordinates <r,t,z>, with t in radians)

Parameter	Value
B2B Throat Length 0	1.22596
Segment 0: 0:(2,0.524617,2.9776) to 0:(2,1.02217,2.26155)	1122553
Crv Throat Length 0	1.22573
LE Pitch	2.0944
TE Pitch (S)	2.0944
Centroid:Z	2.22517
Centroid:R	2
Centroid:T	4.9°
Centroid:Mp	0.362584
Centroid:M	0.725168

Airfoil Area	0.298597

Blade & Layer Parameters (using M vs T-Prime system)

Parameter	Value
3D Meanline Length	2.04173
Camber Length	2.04175
Cord Length (C)	1.83116
Meridional Length (M)	1.5
Stagger Angle	35.0°
Solidity (C/S)	0.874315
Pitch Cord Ratio (S/C)	1.14375

Bezier Parameters:

Standard Parameters:

Parameter	Value
Stagger Angle	35.0°
LE Theta Angle	0.0°
LE Beta Angle	-25.0°
TE Beta Angle	60.0°
LE Wedge Angle	15.0°
TE Wedge Angle	2.0°
LE Thickness	0.1
TE Thickness	0.0399991

Advanced Side1 Point Parameters:

Parameter	Value
First Point %M'	20.0
Last Point %M'	80.0
Linear Point %M'	30.0

Advanced Side2 Point Parameters:

Parameter	Value
First Point %M'	30.0
Last Point %M'	80.0
Linear Point %M'	0.0

Layer: Span: 0.7500

(coordinates shown in cylindrical coordinates <r,t,z>, with t in radians)

Parameter	Value
B2B Throat Length 0	1.44879
Segment 0: 0:(2.25,0.463676,2.9784) to 0:(2.25,1.0101,2.211951	1
Crv Throat Length 0	1.44843
LE Pitch	2.3562
TE Pitch (S)	2.3562
Centroid:Z	2.22456
Centroid:R	2.25
Centroid:T	4.3°
Centroid:Mp	0.322027

Centroid:M	0.724561
Airfoil Area	0.297991

Blade & Layer Parameters (using M vs T-Prime system)

Parameter	Value
3D Meanline Length	2.0363
Camber Length	2.03631
Cord Length (C)	1.8274
Meridional Length (M)	1.5
Stagger Angle	34.8°
Solidity (C/S)	0.775574
Pitch Cord Ratio (S/C)	1.28937

Layer: Span: 1.0000
(coordinates shown in cylindrical coordinates <r,t,z>, with t in radians)

Parameter	Value
B2B Throat Length 0	1.66895
Segment 0: 0:(2.5,0.420312,2.98012) to 0:(2.5,1.00449,2.172351	1
Crv Throat Length 0	1.66857
LE Pitch	2.61799
TE Pitch (S)	2.61799
Centroid:Z	2.22515
Centroid:R	2.5
Centroid:T	3.9°
Centroid:Mp	0.29006
Centroid:M	0.725149
Airfoil Area	0.298618

Blade & Layer Parameters (using M vs T-Prime system)

Parameter	Value
3D Meanline Length	2.04174
Camber Length	2.04174
Cord Length (C)	1.83116
Meridional Length (M)	1.5
Stagger Angle	35.0°
Solidity (C/S)	0.699452
Pitch Cord Ratio (S/C)	1.42969

Bezier Parameters:
Standard Parameters:

Parameter	Value
Stagger Angle	35.0°
LE Theta Angle	0.0°
LE Beta Angle	-25.0°
TE Beta Angle	60.0°
LE Wedge Angle	15.0°

TE Wedge Angle	2.0°
LE Thickness	0.1
TE Thickness	0.0399991

Advanced Side1 Point Parameters:

Parameter	Value
First Point %M'	20.0
Last Point %M'	80.0
Linear Point %M'	30.0

Advanced Side2 Point Parameters:

Parameter	Value
First Point %M'	30.0
Last Point %M'	80.0
Linear Point %M'	0.0